Hamburg University of Applied Sciences

Faculty of Life Sciences

Department of Biotechnology

Investigating the Impact of UVB and Cyclosporin A on Epithelial and Mesenchymal Cell Behavior in Monolayer Culture

Master Thesis

in the study program Pharmaceutical Biotechnology

Elizabeth Bella Agustya

[redacted]

Hamburg, 15.10.2025

First examiner: Prof. Dr Julien Béthune (HAW Hamburg)

Second examiner: Dr. rer. nat. Beate Volkmer (Elbe Klinikum Buxtehude)

This thesis was supervised and prepared in the laboratory for molecular cell biology at the Elbe Kliniken Stade-Buxtehude

Abstract

Cyclosporin A (CsA) is a keystone immunosuppressant used in organ transplantation and autoimmune disease management. However, long-term administration is linked to an elevated risk of cutaneous squamous cell carcinoma (cSCC), particularly in UV-exposed skin. Despite extensive knowledge about its immunoregulatory mechanisms, the direct cellular responses of skin epithelial and stromal cells remain less understood. This study investigated the early molecular and functional effects of CsA, UVB irradiation, and the Akt inhibitor Triciribine (TCN) in two-dimensional (2D) monolayer cultures of HaCaT keratinocytes and dermal fibroblasts.

Gene expression profiling focused on key pathways central to epithelial-mesenchymal transition (EMT), extracellular matrix (ECM) remodeling, and stress signaling. In keratinocytes, CsA enhanced ATF3 expression under UVB and kinase inhibition (TCN), while E-cadherin (CDH1) remained consistently expressed, preserving epithelial identity. Migration assays revealed impaired collective motility, particularly after UVB exposure. Interestingly, CsA appeared to buffer UVB-induced cytotoxicity and detachment, suggesting a partially protective role and potential involvement in counteracting EMT progression during acute stress. In fibroblasts, transcriptional activation of the TGF-β pathway and MMP9 under TCN treatment highlighted early fibroblast activation and dynamic ECM remodeling. Fibroblasts exhibited robust motility and resilience to CsA and UVB, and showed only mild delays after TCN exposure without significant cytotoxicity.

These findings underscore distinct adaptive strategies: keratinocytes prioritize stress adaptation and epithelial preservation, while fibroblasts engage remodeling programs to sustain tissue integrity. Importantly, TCN alone or in combination with UVB and/or CsA, emerged as a key modulator of fibroblast behavior, influencing mesenchymal traits and ECM dynamics. Although 2D assays are limited in fully capturing invasive transformation compared to 3D systems, they effectively reflect early-stage adaptation and cell-matrix interactions under pharmacological and environmental stress. Overall, this work provides new insights into CsA- and UVB-mediated regulation of skin cell behavior, with implication for understanding cSCC development in immunosuppressed patients, and lays the foundation for future studies on chronic adaptation, invasive transformation, and dermal-epidermal dynamics in cancer and wound healing contexts.

Table of Contents

List of Abbreviations

AKT1	RAC-alpha serine/threonine protein kinase 1
AP-1	Activator protein 1
ATF3	Activating transcription factor 3
BCC	Basal cell carcinoma
BR	Broad range
CDH1	E-cadherin
CDH2	N-cadherin
COL7A1	Collagen type VII alpha chain 1
CPD	Cyclobutane pyrimidine dimers
CsA	Cyclosporin A
cSCC	Cutaneous squamous cell carcinoma
DMEM	Dulbecco's modified eagle medium
DMSO	Dimethylsulfoxid
DNA	Deoxyribonucleic acid
dNTP	Deoxynucleotide triphosphates
ECM	Extracellular matrix
EDTA	Ethylenediaminetetraacetate
EGF	Epidermal growth factor
EMT	Epithelial-mesenchymal transition
FBS	Fetal bovine serum
FGF	Fibroblast growth factor
GVHS	Graft-versus-host syndrome
HKG	Housekeeping gene
HPRT1	Hypoxanthine phosphoribosyltransferase 1
IARC	International agency for research on cancer
IGF	Insulin-like growth factor
IR	Infrared
JNK	C-Jun-N-terminal kinase
MAPK	Mitogen-activated protein kinases

MM	Malignant melanoma
MMC	Mitomycin C
MMP	Matrix metalloproteinase
mTOR	Mammalian target of rapamycin
NFATc	Nuclear factor activated T-cell
NGS	Next generation sequencing
NMSC	Non melanoma skin cancer
OTCs	Organotypic cultures
OTR	Organ transplant recipient
PBS	Phosphate-buffered saline
PCR	Polymerase chain reaction
PDK1	3-phosphoinositide-dependent kinase 1
RNA	Ribonucleic acid
ROS	Reactive oxygen species
RPLP0	Ribosomal protein lateral stalk subunit P0
RPMI	Roswell Park memorial institute medium
SCC	Squamous cell carcinoma
SMAD	Suppressor of mother against decapentaplegic
TBP	TATA-binding protein
TCN	Triciribine
TE	TRIS-EDTA
TGF-β	Transforming growth factor-β
TME	Tumor microenvironment
UV	Ultraviolet
ZEB1	Zinc finger E-box binding homeobox 1

List of Figures

List of Tables

1. Introduction

1.1 Skin Anatomy and Function

The skin represents the largest organ of the human body and plays a vital role in maintaining physiological homeostasis, shielding internal organs, and mediating interactions with the external environment[1]. Its complex structure and diverse functions make it the primary barrier against pathogens, physical injury, and harmful environmental factors such as ultraviolet (UV) radiation[2]. The skin contributes to immunological defense by presenting antigens through specialized immune cells within the epidermis. Beyond its barrier function, skin also contributes to thermoregulation, water balance, sensory perception, and the synthesis of essential compounds like vitamin D[1,2].

Structurally, the skin is organized into three interconnected layers: the epidermis, dermis, and hypodermis (subcutaneous tissue) (Figure 1). Each layer is structurally distinct and serves specific physiological functions. As the outermost layer, the epidermis is continuously exposed to the environment and hosts immune cells, resident microbiota, keratinocytes, and pigment-producing melanocytes. Keratinocytes, which make up the majority of cells in the epidermis, undergo constant renewal and provide a critical physical barrier. Beneath the epidermis, the dermis forms a supportive layer characterized by a dense connective tissue framework of collagen and elastin fibers. It also houses essential structures including hair follicles, nerves, vascular networks, and sweat glands. Separating the dermis from the epidermis is the basement membrane (BM), a specialized extracellular matrix enriched in laminin, collagen, and proteoglycans that ensures structural cohesion and signaling between two layers[3]. The deepest layer, hypodermis, is rich in adipose tissue and functions as both an energy reservoir and an insulator[4,5]. Muscles and bone structure are connected to the skin by this layer.

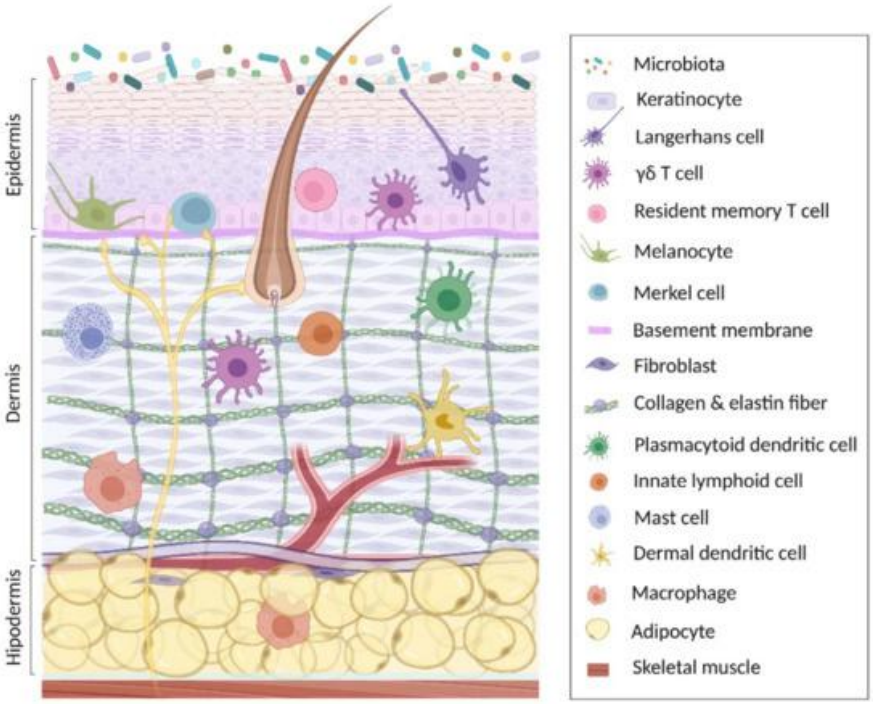

Figure 1: Schematic cross-section of human skin illustrating its three primary layers: epidermis, dermis, and hypodermis. The predominant cellular populations and resident immune cells are presented in each region. Key cellular components include keratinocytes in the epidermis and fibroblasts within the dermis, which collaborate to paracrine signaling to regulate skin homeostasis and repair. Adapted from (Gallegos-Alcalá et al., 2021[6]).

Disruption of skin architecture can significantly affect its form and function, contributing to various pathological conditions, including cancer, through mechanisms such as DNA damage, mutation accumulation, and regulatory imbalance. Both the epidermis and dermis are central to disease processes due to their roles in cell regulation, immune defense, and tissue remodeling. While structural integrity is essential, the skin's regenerative and immunological function are equally dependent on dynamic cellular interactions. A vital component of skin physiology is the extracellular matrix (ECM), primarily synthetized by dermal fibroblasts. These mesenchymal cells are essential for wound healing, fibrosis, and tumor progression. Fibroblasts secrete cytokines, growth factors, and ECM proteins, facilitating intercellular communication and regulating stem cell niches. Their accessibility and adaptability in vitro make them widely used in skin biology research[7,8].

Equally important is the crosstalk between fibroblasts and keratinocytes, particularly during wound healing and inflammation. This interaction is mediated by paracrine signaling loops which modulate keratinocyte behavior. In turn, keratinocytes release signals like interleukin-1 (IL-1), which promote their own migration and proliferation as well as the recruitment of other cells

necessary for tissue repair. As healing progresses, fibroblasts deposit collagen and differentiate into myofibroblasts, contributing to ECM formation and wound contraction[8,9].

Therefore, keratinocyte and fibroblasts are well-established models for studying these interactions. Their use enables controlled investigation of cellular responses to environmental and pharmacological stimuli, including those relevant to skin carcinogenesis and tissue regeneration.

1.2 Skin Cancer Pathogenesis and Risk Factors

Skin cancer is a group of malignant tumors arising from different skin cell types and is the most diagnosed cancer worldwide, with incidence rates steadily increasing, particularly among older adults[10]. It is broadly categorized into malignant melanoma (MM), originating from melanocytes, and non-melanoma skin cancer (NMSC), which develops primarily from epidermal keratinocytes. The main subtypes of NMSC are basal cell carcinoma (BCC), with being the most frequently diagnosed, and cutaneous squamous cell carcinoma (cSCC), which is strongly associated with cumulative UV exposure[11,12]. Additionally, rarer forms such as Merkel cell carcinoma are also recognized[13].

1.2.1 Solar Radiation and Its Role in Skin Carcinogenesis

Solar radiation encompasses a range of electromagnetic waves reaching the earth's surface, including UV, visible, and infrared (IR) light. Among these, UV radiation is the most relevant to skin biology and pathology. It is subdivided by wavelength into UVC (100-280 nm), UVB (280-315 nm), and UVA (315-400 nm). Although UVC is effectively filtered by the stratospheric ozone layer, UVA and UVB penetrate the atmosphere and significantly affect human skin[14,15].

UVB radiation primarily targets the epidermis, inducing direct DNA damage such as cyclobutane pyrimidine dimers (CPDs)[16], which are key contributors to mutagenesis and skin carcinogenesis. In contrast, UVA penetrates deeper into the dermis, generating reactive oxygen species (ROS) that cause oxidative stress[17], resulting in indirect DNA damage, photoaging, and alterations in pigmentation and skin elasticity.

Both UVA and UVB are classified as group 1 carcinogens by the international Agency for Research on Cancer (IARC), with strong evidence linking them to BCC, cSCC, and MM. Their carcinogenicity arises from combined mutagenic effects and immunosuppressive mechanisms that

disrupt epidermal immune surveillance. Artificial UV sources, such as tanning beds, pose similar risks, especially with prolonged exposure[12,14,18].

Despite these risks, UV radiation also plays essential physiological roles. Moderate UVB exposure is necessary for the photochemical synthesis of vitamin D3, which supports calcium metabolism, bone health, and immune regulation[12]. Study research suggests additional systemic benefits, such as nitric oxide-mediated blood vessel widening, which may contribute to blood pressure regulation[19,20]. Clinically, controlled UV therapies, such as narrowband UVB and UVA1 phototherapy, are employed to treat inflammatory skin disorders by harnessing UV's immunosuppressive and anti-inflammatory properties[21,22].

Nevertheless, chronic or excessive exposure to UV and IR radiation contributes to cumulative skin damage, including photoaging, fibrosis, and increased risk of ocular diseases such as cataracts[23]. The link between UV exposure and skin cancer is particularly evident in cSCC, which commonly arises on chronically sun-exposed skin in older individuals, with an average patient age of around 76 years[24]. This underscores the role of accumulated UV-induced genetic damage in its development[12,25]. Although melanoma is less frequent, it is more aggressive and prone to metastasis[14,19,25]. Conversely, among NMSC, cSCC has a lower case-specific mortality rate but contributes to a comparable number of deaths due to its high incidence compared to BCC[26]. Genetically, cSCC exhibits about three times more mutations than melanoma, reflecting its stepwise development from precursor lesions such as actinic keratosis and SCC in situ[26,27]. A frequent mutation observed in about half of cSCC cases is the inactivation of the tumor suppressor gene p53, a key event in the progression of invasive cancer[28].

Altogether, solar radiation represents a dual-edged environmental factor for human health. While essential for vitamin D synthesis and harnessed in therapeutic contexts, its UV components, particularly UVA and UVB, are major drivers of cutaneous carcinogenesis. Their capacity to induce both direct DNA damage and indirect oxidative stress, combined with their immunosuppressive effects, underscores their central role in the development of skin cancer, especially cSCC.

1.2.2 Immunosuppression and Skin Cancer Susceptibility

Immunosuppression is strongly linked to an increased risk of cSCC, particularly among organ transplant recipients (OTRs) who receive long-term immunosuppressive treatment[29,30]. Numerous studies have shown that immunosuppression acts as an independent risk factor for cSCC, often resulting in more aggressive, multifocal disease and poorer clinical outcomes[31]. Importantly, UV radiation is the primary environmental driver of DNA damage in the skin, inducing characteristic lesions such as CPDs. If unrepaired, these lesions can result in mutations promoting oncogenic transformation. Immunosuppression further increases this risk by impairing immune surveillance mechanisms that would otherwise eliminate UV-damaged cells. In addition to its systemic effects, immunosuppressive therapy has been shown to exert direct effects on keratinocytes, including the activation of oncogenic signaling pathways and inhibition of DNA repair processes, independent of immune suppression[32–34]. This interplay highlights the critical role of UV exposure and immune regulation in the pathogenesis of cSCC in immunosuppressed individuals.

Cyclosporin A (CsA) is a calcineurin inhibitor widely prescribed to prevent graft rejection and manage autoimmune diseases. Its primary mechanism of action is the inhibition of calcineurin, a calcium-dependent phosphatase essential for activating nuclear factor of activated T-cells (NFAT). Under normal conditions, calcineurin dephosphorylates NFAT, allowing it to translocate into the nucleus and initiate transcription of genes necessary for T-cell activation[35]. CsA exerts its immunosuppressive effects by forming a complex with cyclophilin-A (an immunophilin) that binds and inhibits calcineurin, thereby blocking NFAT activation, subsequent T-cell activation, and cytokine production[36–38] (Figure 2).

Beyond this calcineurin-dependent pathway, CsA also impacts immune responses through calcineurin-independent mechanisms. It inhibits signaling pathways such as c-Jun N-terminal kinase (JNK) and p38 MAP kinase, suppressing the activation of transcription factors like AP-1[39]. It blocks upstream components of the MAPKKK (MAPK kinase kinase) cascade, thereby suppressing JNK and p38 activation without affecting extracellular signal-regulated kinase (ERK) signaling[40]. CsA further upregulates transforming growth factor-beta (TGF-β)[41], a cytokine with strong immunosuppressive effects that also promotes extracellular matrix (ECM) protein deposition and tissue fibrosis. While these effects are beneficial for graft tolerance, long-term CsA use has been associated with an increased incidence of malignancies, including cSCC, due to

impaired immune monitoring and potential direct pro-tumorigenic effects like migration and invasion in epithelial cells of the skin[42–44]. Thus, CsA's broad inhibition of immune signaling illustrates the complex balance of immunosuppressive therapies, which can both suppress immune function and promote carcinogenesis in the skin.

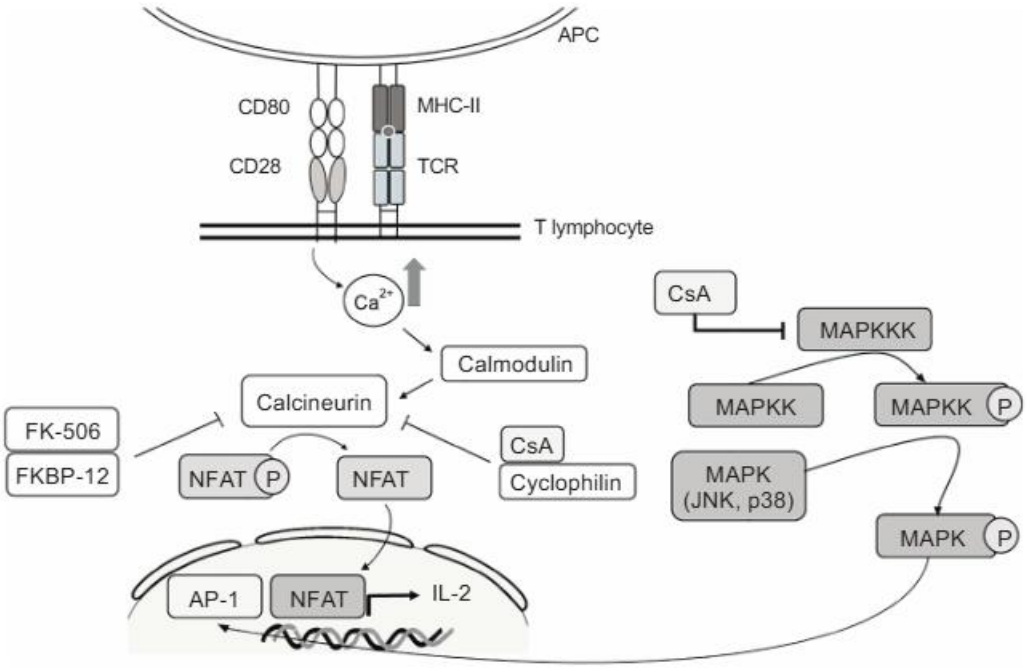

Figure 2: Schematic of calcineurin inhibitor pathways. Upon T-cell activation, calcium influx activates calcineurin, a phosphatase that dephosphorylates NFAT family members, enabling their nuclear translocation and transcriptional activation of genes such as interleukin-2 (IL-2), which is essential for full T-cell activation. CsA and tacrolimus (FK506) exert immunosuppressive effects by forming complexes with their respective immunophilins (cyclophilin and FKBP) that directly inhibit calcineurin activity. In addition to blocking NFAT signaling, CsA also interferes with MAPK pathways, particularly JNK and p38, by inhibiting their phosphorylation. This prevents activation of transcription factors such as AP-1, further contributing to suppression of IL-2 expression and immune responses. Adapted from (Lee et al.,2023[40])

Clinical observations indicate that discontinuation of CsA and replacement with alternative immunosuppressant often reduces the incidence of cSCC[45]. Tacrolimus, another calcineurin inhibitor with a more favorable graft survival profile, is frequently used as an alternative. However, Tacrolimus also carries risks, including promotion of skin carcinogenesis and a potential association with post-transplant cognitive dysfunction[46,47], necessitating careful long-term risk benefit evaluation.

1.3 Cellular Plasticity and Stress Responses in Skin Cells

The skin's layered architecture, comprising the epidermis and dermis, reflects a complex interplay between epithelial and mesenchymal cell types. These layers respond distinctly to environmental and pharmacological stressors, yet their coordinated behavior is essential for maintaining tissue integrity and responding to injury. To investigate stress responses in vitro, both 3D organotypic cultures (OTCs) and 2D monolayer cultures are considered as suitable models. While 3D OTCs offer a more physiologically relevant model, 2D systems allow for precise dissection of early cellular responses, particularly those related to plasticity and stress signaling.

1.3.1 Epithelial Plasticity: EMT in Keratinocytes

Epithelial-mesenchymal transition (EMT) is a reversible biological process where epithelial cells lose their characteristic polarity and intercellular adhesion, acquiring a mesenchymal phenotype that enhances motility, invasiveness, and resistance to cell death. This transformation allows epithelial cells to migrate and remodel tissues, playing crucial roles in embryonic development, wound healing, and pathological conditions such as fibrosis and cancer progression[48–50].

In skin tissue, EMT supports normal tissue repair but also contributes to malignant progression by promoting invasive behaviors in keratinocytes. The initiation of EMT is strongly influenced by external stimuli from the tumor microenvironment (TME), which comprises fibroblasts, immune cells, endothelial cells, and adipocytes within the extracellular matrix (ECM)[51]. During this process, epithelial characteristics are progressively lost, as reflected by decreased E-cadherin expression, while mesenchymal markers such as Vimentin and N-cadherin expression are gained. These alterations drive reorganization of the cytoskeleton, facilitate ECM degradation and enhance invasion[52]. In the context of cancer, this process is co-opted by tumor cells to increase their invasive and metastatic potential (Figure 3).

EMT is regulated by diverse extracellular signals, including inflammatory cytokines and growth factors such as transforming growth factor-beta (TGF-β), epidermal growth factor (EGF), insulin like growth factor (IGF), and fibroblasts growth factors (FGFs). Among these, TGF-β plays central role by activating intracellular signaling pathways that disrupt cell-cell junctions, remodel the actin cytoskeleton, and promote the formation of migratory structures such as filopodia and lamellipodia. Additionally, matrix metalloproteinases (MMPs) further support this process by degrading the

basement membrane, facilitating cellular detachment and invasion. In skin cancer, EMT contributes to the acquisition of mesenchymal traits, enabling tumor cells to invade neighboring tissues and metastasize to distant organs[50,52–54].

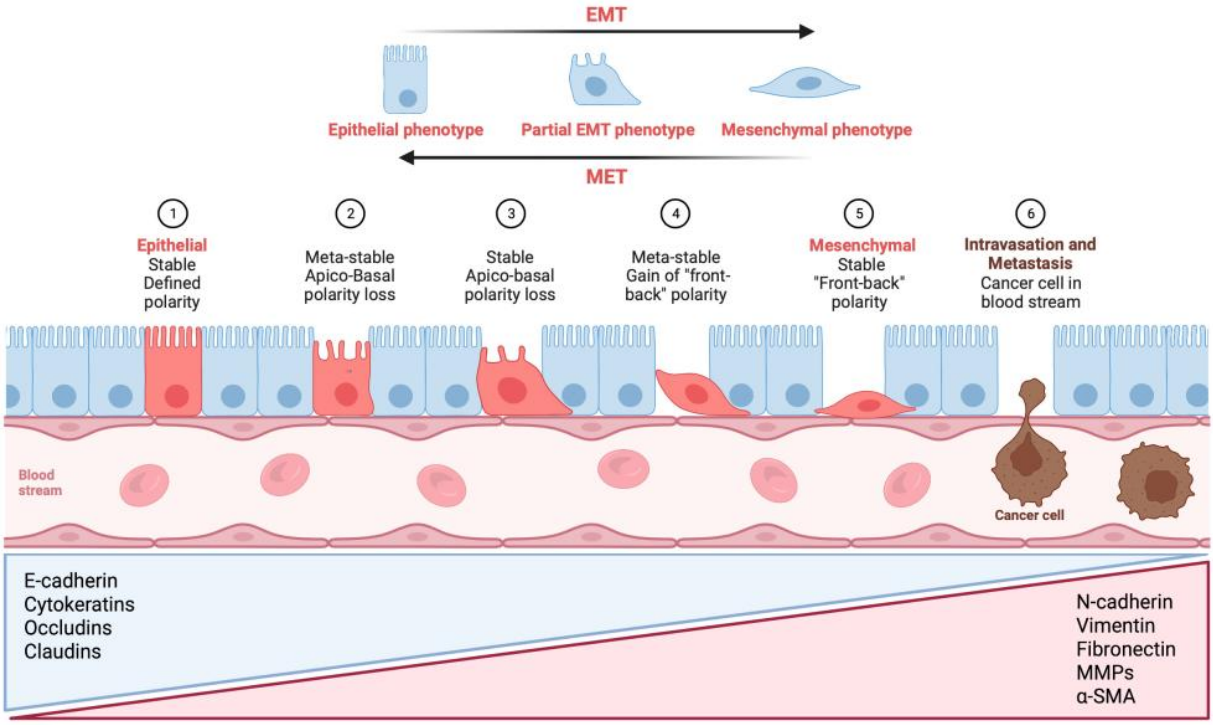

Figure 3: Schematic representation of EMT. Epithelial cells, characterized by apical-basal polarity and adhesion molecules (e.g., E-cadherin), progressively lose their traits and acquire mesenchymal features such as front-back polarity, cytoskeletal reorganization, and expression of markers like N-cadherin and Vimentin. This transition enhances cell migration, invasion, and stem-like properties, contributing to metastasis and treatment resistance. EMT is reversible through mesenchymal to epithelial transition (MET), which supports metastatic colonization and tumor expansion. Adapted from (Hoch et al.,2023[55])

Environmental stressors like UV radiation can induce EMT-related responses via oxidative stress and inflammatory signaling. In the context of immunosuppressive treatment, CsA has been shown to induce EMT-like features in keratinocytes, increasing their invasive behavior in OTCs[56,57]. This effect is partly mediated by activation of the PI3K/Akt signaling pathway. Pharmacological inhibition of Akt with triciribine (TCN) effectively reduces CsA-induced invasion[38,58], however, concurrent UV exposure reverses this inhibition, suggesting a complex interaction where UV stress can overcome pathway blockade and restore invasive EMT behaviors.

1.3.2 Mesenchymal Remodeling: Fibroblasts Responses to Stress

Fibroblasts are the principal mesenchymal cells of the dermis, responsible for synthesizing and remodeling ECM components, maintaining skin integrity, and facilitating wound healing. Unlike

keratinocytes, fibroblasts do not undergo EMT but exhibit plasticity through dynamic changes in gene expression, migratory behavior, and cytokine secretion, allowing them to respond rapidly to injury or environmental insults such as UV radiation[7,9]. Fibroblasts can therefore serve as a model to understand how non-epithelial cells contribute to tissue remodeling and tumor-supportive microenvironments under stress conditions.

In pathological contexts, fibroblasts can be activated by paracrine signals from keratinocyte, immune cells, or tumor cells, transforming into cancer-associated fibroblasts (CAFs). CAFs contribute to tumor progression, invasion, and the formation of supportive microenvironment, facilitating cancer growth and metastasis[7,59–61] (Figure 4).

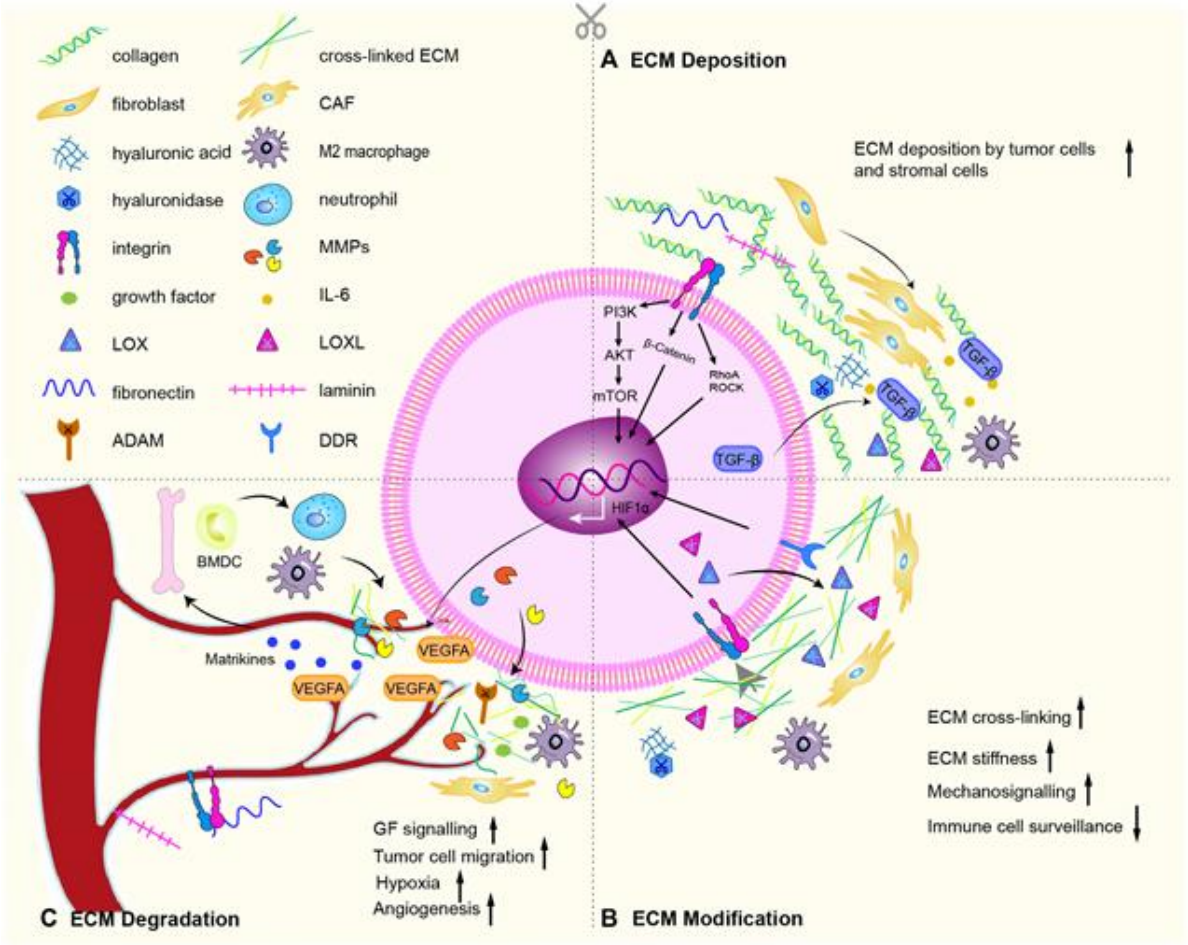

Figure 4: Mechanisms of ECM remodeling by fibroblasts. (A) Cancer-associated fibroblasts (CAFs), activated primarily via TGF-β signaling, deposit abundant ECM components such as collagen, fibronectin, hyaluronic acid, and laminin. They also secrete cytokines that recruit and activate M2 macrophages, contributing to an immunosuppressive microenvironment. (B) chemical and mechanical modifications of the ECM alter its biochemical properties and structural organization. Enzymes such as lysyl oxidase

(LOX) and LOX-like proteins increase ECM stiffness and fibrosis, promoting tumor progression. Mechanical forces mediated by integrins and DDR align ECM fibers and open migration channels, facilitating cancer cell invasion. (C)CAFs, tumor cells, and bone marrow-derived cells (BMDCs) secrete proteases-including MMPs, ADAMs, and disintegrins, that degrade ECM components. This degradation releases matrix-bound growth factors and bioactive fragments (matrikines), which enhance tumor proliferation, migration and invasion. Neutrophils recruited by matrikines further release MMP9, delivering vascular endothelial growth factor (VEGF) and promoting vascular sprouting. In dense ECM conditions, tumor cells may acquire endothelial-like properties and mimic vascular structures. Modified and adapted from (Liang, et al.2023 and Winkler et al. 2020[62,63])

1.4 Target Genes and Their Functional Roles

This study investigates a panel of 13 genes central to the regulation of EMT (CDH1, CDH2, ZEB1), ECM remodeling (MMP2, MMP9, COL7A1), cell survival and signal transduction (AKT1, NFATc1, ATF3, TGFB1, SMAD2/3/4), which are important in skin development, wound healing activity, and tumor progression. AKT1 encodes protein kinase B that regulates cell proliferation, survival, and migration. Its activation is strongly associated with increased tumor growth, metastatic capacity, and resistance to apoptosis, primarily through downstream mTOR signaling[64–66]. NFATc1 (nuclear factor of activated T-cells, cytoplasmic 1) is a transcription factor essential for T cell activation and skin inflammation. It modulates genes involved in immune responses, and keratinocyte proliferation, contributing to skin homeostasis[67,68]. ATF3 (activating transcription factor 3) is a stress response transcription regulator involved in cell cycle arrest and apoptosis. It is rapidly induced by DNA damage, wounding, and inflammatory signals, balancing cell proliferation and survival[69,70]. CDH1 and CDH2 encode E-cadherin and N-cadherin, molecules that maintain epithelial integrity (CDH1) or drive the mesenchymal phenotype and migratory behavior (CDH2). During EMT, CDH1 is typically downregulated and CDH2 is upregulated, marking the transition crucial for cancer invasion and metastasis[71,72]. ZEB1 (zinc finger E-box binding homeobox 1) is a transcriptional repressor that directly suppresses epithelial markers like E-cadherin, driving EMT and promoting cell plasticity, migratory potential, and invasion during tumor progression[73,74]. MMP2 and MMP9 are matrix metalloproteinases responsible for degrading extracellular matrix components, facilitating cell migration and tissue remodeling. Elevated MMP2/9 expression correlates with increased invasiveness in many malignancies and is central to tumor metastasis[75,76]. COL7A1 encodes type VII collagen, a structural protein forming anchoring fibrils at the dermal-epidermal junction, essential for skin integrity. Loss or mutation of COL7A1 disrupts this barrier[77]. TGFB1 (transforming growth factor-beta 1) is a multifunctional cytokine that organizes EMT, fibrosis, and immunosuppression. It promotes ECM production and the differentiation of fibroblasts and myofibroblasts[78]. TGFB is also known for its dual role in cancer, functioning as a tumor suppressor by inhibiting cell proliferation and promoting differentiation in

early stages, but switching to a tumor promoter in later stages by enhancing invasion and metastasis[79]. SMAD2, SMAD3, SMAD4, are intracellular mediators of TGF-β signaling. Following ligand stimulation, SMAD2/3 associated with SMAD4 and move into the nucleus, where they regulate the transcription of EMT, proliferation, and differentiation related genes, central to cancer development and immune modulation[80] (Figure 5).

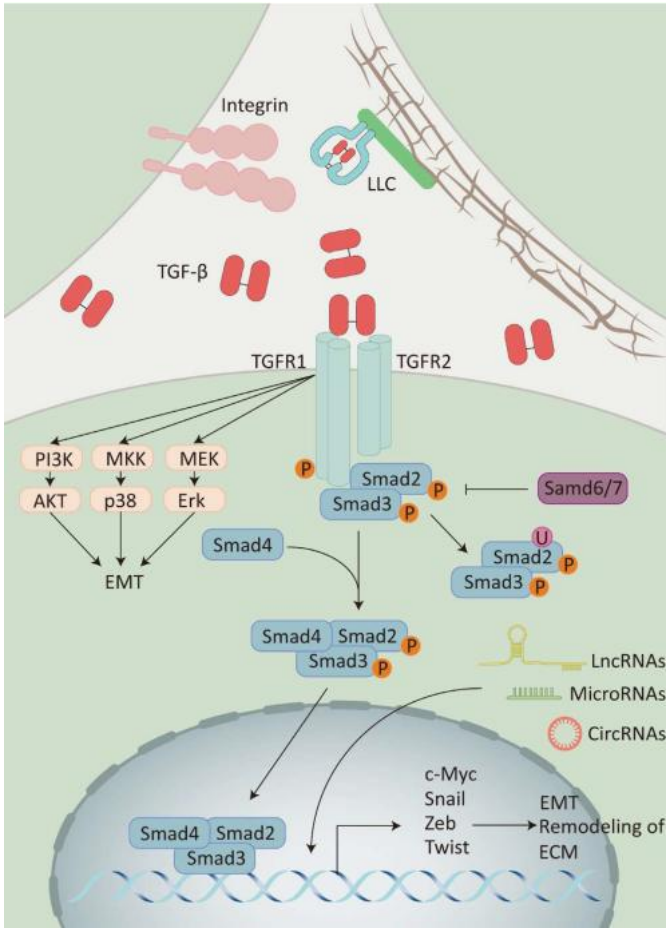

Figure 5: Overview of TGF-β signaling in EMT and ECM remodeling. TGF-β is released from the ECM via integrin-mediated activation (LLC) and initiates signaling by binding to its receptors (TGFRI/II). This activates receptor-regulated SMADs (SMAD2/3), which form a complex with SMAD4 to regulate target gene expression. Inhibitory SMADs (SMAD6/7) can block this pathway. Beyond the canonical SMAD-dependent route, TGF-β also engages non-canonical pathways such as PI3K/AKT, p38 MAPK, and ERK, contributing to cellular plasticity and matrix remodeling. Additionally, non-coding RNAs modulate TGF-β signaling by influencing transcription factor activity and gene expression. Adapted from (Liao et al., 2024[81]).

1.5 Aim of the Study

Cyclosporin A (CsA) has revolutionized transplant medicine by significantly improving graft survival and remains a key treatment for autoimmune diseases and graft-versus-host syndrome (GVHS). However, its long-term use is associated with a heightened risk of cutaneous squamous cell carcinoma (cSCC), particularly in organ transplant recipients (OTRs) with significant sun exposure. While CsA's immunosuppressive efficacy is well established, emerging evidence suggests that its tumor-promoting actions appear to be localized to the skin and can be independent of systemic immune modulation.

To address the possible mechanisms of CsA-associated cSCC development, a recent study using 3D OTC model demonstrated that CsA promotes tumor-like invasion in long-term human skin equivalents[38]. The present investigation focuses on short-term cellular responses in two-dimensional (2D) monolayer cultures of HaCaT keratinocytes and dermal fibroblasts. Culturing these cell types separately under identical treatment conditions enables a more direct assessment of CsA's non-immunological effects on skin cell behavior. Triciribine (TCN), an Akt pathway inhibitor, was included to investigate the role of survival signaling in CsA-induced modulation.

To further explore environmental co-factor fundamental to skin carcinogenesis, UVB irradiation, a known inducer of DNA damage and skin cancer, was incorporated into the experimental design. A UVB source corresponding to solar-UVB radiation was used to mimic UVB exposure and assess potential synergistic effects between CsA and UVB in modulating cell migration, gene expression, and epithelial integrity.

The primary aim of this study is to elucidate the early molecular and cellular changes induced by CsA, TCN, and UVB in 2D skin monolayer cultures. By analyzing the expressions of key genes involved in epithelial-mesenchymal transition (EMT), extracellular matrix (ECM) remodeling, and stress signaling via qPCR, alongside functional migration assays, this work seeks to clarify CsA's contribution to skin carcinogenesis beyond immune suppression. The results obtained in this study will be compared with findings from 3D models to provide a more comprehensive understanding. Finally, the findings aim to better understand the underlying molecular mechanisms that may inform the development of therapeutic strategies to minimize adverse outcomes.

2. Materials and Methods

2.1 Materials

2.1.1 Devices

Table 1 Devices

Device	**Manufacturer**	**Series**
Analytical balance	Kern & Sohn	870-61
Aspirator	Weinmann	Accuvac Basic E341
Centrifuge	Hettich	Mikro 200
Centrifuge	Hettich	Universal 320
CO_2 incubator	Binder	CB 210
Freezer (-20°C)	Liebherr	Comfort 461724
Freezer (-70°C)	Sanyo	T1992
Fridge (4°C)	Bosch	KTR
Fume hood	Köttermann	7590
Ice machine	Hoshizaki	Scotsman AF100
Light microscope	Olympus	CKX53
Pipetting aid	Hirschmann	Pipettus-Accu
Shaker	Heidolph	Rotamax 120
Sterile work bench class 2	Flow laboratories	Gelaire BSB-4A
Thermocycler	Analytik Jena	qTower^3 G touch
UV irradiation lamp	KAUVIR consortium	KAUVIR
Vacuum pump	Weinmann	Accuvac Basic
Vortexer	IKA Laboratory	Vibrofix VF2
Water bath	GFL	GFL 1083

2.1.2 Consumables

Table 2 Consumables

Product	Manufacturer
24 well plate	Greiner Bio-One
Cell culture dishes (35 mm, 60 mm)	Greiner Bio-One
Cell culture flask T75	Greiner Bio-One
Cell scraper	Greiner Bio-One
CellStar centrifuge tubes	Greiner Bio-One
Centrifuge tubes (15mL, 50mL)	Greiner Bio-One
Cuvette	Carl Roth GmbH
Disposable syringe (5mL, 10mL)	Becton, Dickinson, and Company
Forceps	Carl Roth GmbH
Freezing container, Mr. Frosty	VWR
Freezing tubes (1mL)	Greiner Bio-One
Neubauer hemocytometer	Karl Hecht GmbH
Parafilm	Bemis, Inc
PCR strips	Greiner Bio-One
Petridish (Ø 60 mm, 35 mm)	Greiner Bio-One
Pipette tips	Ratiolab GmbH
Pipettes	Eppendorf
Reaction tubes	Greiner Bio-One
Sterile filter	Merck Millipore
Syringe	Becton Dickinson GmbH

2.1.3 Chemicals and Reagents

Table 3 Chemicals, buffers and reagents

Product	Manufacturer
Chloroform/Trichloromethane (99%)	Carl-Roth GmbH
Cyclosporin A, Calbiochem	Merck
Dimethylsulfoxid (DMSO)	Carl-Roth GmbH

Dulbecco's modified eagle medium (DMEM)	Sigma-Aldrich
EDTA titriplex III (99%)	Merck
Ethanol (100%)	Lohmann
FBS CP18-2361	Capricorn
Methanol	Carl Roth GmbH
Mitomycin C	Sigma-Aldrich
Phosphate-buffered saline (PBS)	Invitrogen
Roswell park memorial institute medium (RPMI)	Gibco Life Technologies
TE Buffer (100x)	Carl Roth GmbH
Trypsin	Biochrom GmbH
Triciribine	Sigma-Aldrich
Water, nuclease free	Carl Roth GmbH

2.1.4 Cell Culture Media and Solutions

Table 4 Composition of cell culture media and solutions

Solutions	**Composition**
DMEM	13.38 g DMEM powder, 3.7 g/L $NaHCO_3$, 100 µg/mL streptomycin, 1000 mL aqua dest, pH 7.3
Freezing media	70% FBS-free medium, 20% FBS, 10% DMSO
RPMI	500 mL RPMI-1640, 5 mL Pen/Strep, 23.8 mM $NaHCO_3$
Trypsin/EDTA (0.25%/0.02%)	0.25 g Trypsin, 0.02 g EDTA, 10 mL $PBS^{-/-}$, pH 7.5

2.1.5 Kits

Table 5 Kits

Name	**Cat. #**	**Manufacturer**
Lexogen SPLIT RNA Extraction Kit	008	Lexogen GmbH
SensiFAST cDNA Synthesis Kit	BIO-650530	Bioline GmbH
Sensimix™ SYBR No-ROX Kit	QT650-05	Bioline GmbH
Qubit™ RNA BR Assay	Q10210	Thermo Fischer

2.1.6 mRNA Primers for qPCR analysis

Primer sequences were obtained from previous studies or designed internally. All primers (Biomers.net) were dissolved in 1x TE buffer and combined (forward and reverse) at equimolar concentrations to a final working solution of 3 µM.

Table 6 mRNA primer sequences

Gene	Sequence 5'→3'	Accession	Amplicon [bp]
AKT1	F: CAGGATCCATGGGTAGGAACA	NM_001382430.1	20
	R: TGGCCACAGCCTCTGATG		25
ATF3	F: CGGAGCCTGGAGCAAAATG	NM_001674.4	19
	R: CTTCCTTGACAAAGGGCGTC		20
CDH1	F: AAGGTGAGGGGTTAAGCACA	NM_004360.5	20
	R: ACCTGACCCTTGTACGTGGT		20
CDH2	F: GGCTTCTGGTGAAATCGCAT	NM_001792.5	20
	R: TGCAGTTGCTAAACTTCACATTG		23
COL7A1	F: TGGTGACAAGGGCAGCAA	NM_000094.4	18
	R: CAGGCACTCCATCCTTTCCT		20
HPRT1	F: TGACACTGGCAAAACAATGCA	NM_000194.3	21
(HKG)	R: GGTCCTTTTCACCAGCAAGCT		21
MMP2	F: CTGAGGGCGCTCTGTCTC	NM_004530.6	18
	R: AAGGTGTTCAGGTATTGCACTG		22
MMP9	F: GCGCTGGGCTTAGATCATTC	NM_004994.3	20
	R: GTTCAGGGCGAGGACCATAG		20
NFATc1	F: ATGCCAAGCACCAGCTTTC	NM_001278669.2	19
	R: GCATAGCCATAGTGTTCTTCCT		22
RPLP0	F: GCGTCCTCGTGGAAGTGAC	NM_001002.4	19
(HKG)	R: TAGTTGGACTTCCAGGTCGC		20
SMAD2	F: GTTTTCAGTTCCGCCTCCAA	NM_005901.6	20
	R: AGCCTCTTGTATCGAACCTGC		21

SMAD3	F: GGTCAAGAGCCTGGTCAAGA	NM_005902.4	20
	R: CATCCAGGGACCTGGGGA		18
SMAD4	F: CTTTGAGGGACAGCCATCGT	NM_005359.6	20
	R: TACTGGCAGGCTGACTTGTG		20
TBP	F: TTCGGAGAGTTCTGGGATTGTA	NM_003194.5	22
(HKG)	R: TGGACTGTTCTTCACTCTTGGC		22
TGFB1	F: TACCTGAACCCGTGTTGCTC	NM_000660.7	20
	R: TTGCTGAGGTATCGCCAGGAA		21
ZEB1	F: CAGAGGATGACCTGCCAACA	NM_001174096.2	20
	R: TTGCCCTTCCTTTCCTGTGTC		21

2.1.7 Primer Design Tools

Table 7 URL for primer design

URL
https://www.ncbi.nlm.nih.gov/tools/primer-blast/
https://www.ensembl.org/index.html
https://www.biosyn.com/gizmo/tools/oligo/oligonucleotide%20properties%20calculator.htm

2.1.8 Software

Table 8 Software

Software	**Developer**
EHDView	EHD imaging GmbH
ImageJ v1.54g	Wayne Rasband
Ms. Office	Microsoft corporation
qPCRSoft 4.1	Analytik Jena

2.1.9 Cell Lines

HaCaT cell line (human, adult, low calcium, high temperature) and human dermal fibroblasts (Fib 44/07; donor no. 44, year 2007; provided by Prof. Dr. P. Boukamp) were utilized in this study. HaCaT is a spontaneously immortalized keratinocyte cell line derived from adult human skin. It exhibits characteristics typical of basal epidermal keratinocytes, including stable growth in standard culture conditions and a non-tumorigenic phenotype in vivo. The cell line carries UV-specific mutations in both alleles of the p53 gene and displays a monoclonal origin marked by unique stable chromosomes[82]. HaCaT cells were used at passages 42-44 for gene expression analysis and at passage 48 for migration assays.

The Fib 44/07 cells represent the dermal compartment and were cultured to model mesenchymal cell behavior. Human dermal fibroblasts play a central role in ECM synthesis and remodeling, wound repair, and paracrine signaling within the skin microenvironment. Fibroblasts exhibit dynamic plasticity in response to environmental and pharmacological stressors, making them a relevant model for studying stromal activation, fibrosis, and ECM-related gene regulation. Fibroblasts were used at passages 10-12 for gene expression analysis and at passage 14 for migration assays.

2.2 Methods

2.2.1 Cell Culture

The entire cell culture procedure was conducted in the biosafety level S1 laboratory, utilizing sterile workbenches throughout the process. To achieve optimal growth conditions, cells were cultured at a temperature of 37°C within an incubator that provided an atmosphere of 5% CO_2 and 95% humidity. The culture medium was changed every two to three days. The medium and other solutions were continually stored in the refrigerator at 4°C and subsequently stabilized in a water bath at 37°C prior to use.

2.2.1.1 Cell Thawing

Frozen cells vial was extracted from a liquid nitrogen storage container. The cells were prepared for thawing in a water bath maintained at 37°C for approximately two minutes or until they reached a state of complete defrosting. Subsequently, cells were inoculated into a T75 flask containing 15

mL of pre-warmed DMEM. On the following day, the medium in the flask was changed with fresh medium to eliminate any residual DMSO that may have been present in the freezing media.

2.2.1.2 Cell Detachment and Plating

Following thawing and initial recovery, cells were cultured in T75 flasks until reaching approximately 80% confluence. For experimental use, cells were detached by aspirating the medium and rinsing with 5 mL $PBS^{-/-}$ to remove residual DMEM. Trypsinization was performed by adding 1.5 mL trypsin/EDTA and incubating at 37°C for 5-10 minutes. Detached cells were dispersed by gentle tapping or pipetting, and the enzymatic reaction was neutralized with 8.5 mL DMEM containing FBS. Cell counts were determined using a Neubauer chamber.

Cells were then seeded onto petri dishes (Ø 60 mm, 35 mm) according to experimental requirements, with DMEM added beforehand to ensure viability. Weekly passaging was performed, and passage numbers were recorded. After treatment completion, cells were detached by aspirating the medium and applying 0.5 mL trypsin/EDTA. Dishes were tapped or scraped to facilitate detachment, and cells were collected and dispersed by pipetting. The reaction was halted with fresh DMEM, and the suspension was centrifuged at 200 x g for 10 minutes. Cells pellets were washed with $PBS^{-/-}$ and prepared for downstream analysis.

2.2.2 Cells Treatments

HaCaT keratinocytes and fibroblasts were seeded in medium containing 1 µM CsA as the working concentration, prepared from a 1 mM stock solution dissolved in 100% DMSO. The Akt inhibitor triciribine (TCN) was added 24 hours after seeding to the cells at a final concentration of 1 µM. After an additional 24 hours, the cultures were exposed to UVB radiation. For negative controls, an equivalent volume of DMSO was added to the medium in place of CsA. Cells in the DMSO control group underwent the same treatment protocol with TCN addition and UV irradiation.

2.2.3 Cells Irradiation

Cells irradiation was performed using a custom-built solar simulator (KAUVIR), designed to deliver controlled exposure to specific components of the solar spectrum (Figure 6). The device allows for combined or individual irradiation with UVA, UVB, infrared-A (IR-A), and visible light (VIS), using independently regulated lamps, dichroic mirrors, and selective optical filters to

achieve spectral compositions closely resembling natural sunlight[83]. For the present study, only UVB source was utilized.

The UVB emission was generated using Philips PL-S 9W/12 2P broadband tubes and filtered to restrict output to the biologically relevant range of 280-315 nm. A combination of long-pass and short-pass filters was employed to eliminate UVC and UVA contamination, ensuring precise spectral targeting. The resulting UVB irradiance was approximately 0.64 ± 0.5 W/m^2, corresponding to 94% of the ASTM G173 reference solar spectrum. Spectral calibration was performed before each experiment using a CCD array spectrometer to maintain consistent output and compensate for lamp aging.

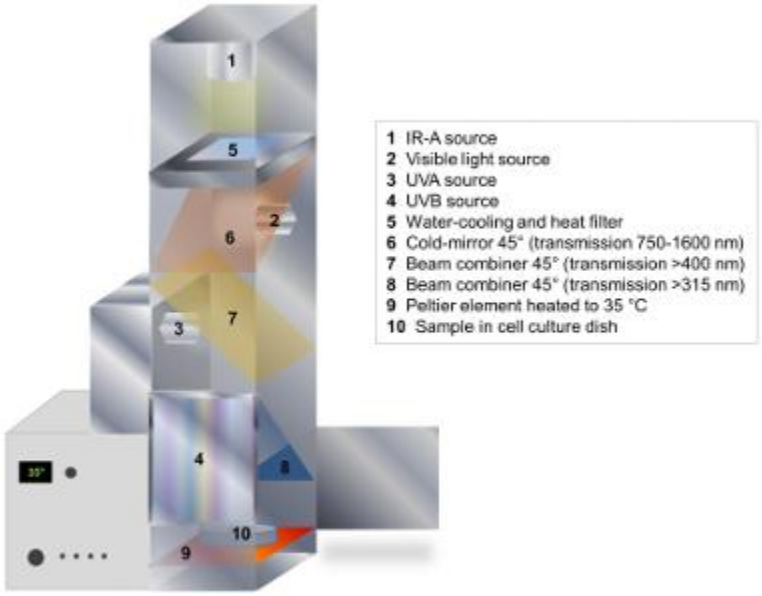

Figure 6: Visualization of the irradiation device. The solar simulation lamp combines IR-A, visible light, UVA, and UVB sources, with irradiance levels resembling natural sunlight. Dichroic beam combiners and optional filters were used to direct light from individual lamps. Samples were placed centrally on a heated Peltier element at the base of the device[83].

For the irradiation experiments, cells were cultured and treated in 60 mm petri dishes until they reached a confluent state. Prior to irradiation, the culture medium was removed, and the cells were gently washed with 5 mL of PBS$^{-/-}$. Subsequently, 3 mL of PBS$^{-/-}$ was added to each dish to maintain hydration, as PBS minimally absorbs UVB. Up to four petri dishes were placed simultaneously on the Peltier-cooled stage of KAUVIR. To minimize interference, petri dish lids were removed during UVB exposure, ensuring accurate dose delivery. Control samples underwent the same preparation steps but were incubated at 35°C in the absence of light for the duration of

the irradiation procedure. The irradiation time was 386 seconds (6 minutes 26 seconds), during which the cells were exposed to a total physical irradiance of 0.647 W/m^2.

Following irradiation, $PBS^{-/-}$ was removed, and 5 mL of the respective growth medium (DMEM/RPMI) was freshly added again to each dish. The cells were then returned to incubation until further treatment or being harvested for further analysis.

2.2.4 Scratch Assay

In monolayer cultures, the scratch assay is a frequently employed method for evaluating the wound healing capacity and cell migration. This investigation involved an assessment of the immunosuppressant effect conducted 72 hours post-seeding. In order to mitigate the impact of cell proliferation on the process of area closure, confluent cell monolayers underwent incubation for 2 hours with Mitomycin C at a concentration of 10 µg/mL in complete medium. Mitomycin C is a cytostatic antibiotic sourced from *Streptomyces caespitosus*, known for its ability to induce covalent cross-linking of DNA strands, thereby inhibiting DNA replication and transcription. Consequently, any noted gap closure can be solely attributed to cell migration, excluding any influences from proliferation[84].

A linear scratch was introduced into the cell monolayer utilizing a 100 µL pipette tip, followed by the removal of cell debris through a double wash with $PBS^{-/-}$. The process of cell migration was systematically observed and recorded using a light microscope at baseline directly after scratch, as well as at 6 hours and 24 hours.

2.2.5 RNA Isolation and Purification

Total RNA was isolated using the Lexogen SPLIT RNA extraction kit. Cell pellets were lysed in the SPLIT lysis buffer and homogenized by pipetting. Lysates were transferred to Phase-Lock Gel tubes and mixed with the phenol-based separation solution. The implementation of these tubes reduces the contamination possibility of the upper phase with the lower phenol phase that includes DNA and proteins. Following centrifugation, the upper aqueous phase containing RNA was carefully collected and applied to the SPLIT spin columns. RNA bound to the membrane was washed sequentially with the supplied wash buffers to remove impurities. Finally, RNA was eluted in 25µL RNase-free water for quantification.

2.2.6 RNA Quantification

The concentration of RNA was determined using the Qubit RNA BR assay kit. The procedure requires the use of two standards. The effective approach involved diluting the BR reagent buffer at a ratio of 1:200. For each sample, 2 µL of the sample was introduced into the appropriate tube. The sample was subsequently vortexed and allowed to incubate for 2 minutes. The Qubit® 2.0 fluorometer was employed to analyze the samples and standards. The sample tube was positioned within the sample chamber, and data was automatically retrieved from the device. Upon reading, the tube was removed, and concentration was given. The isolated RNA is suitable for subsequent analysis through qPCR or NGS to investigate genetic expression.

2.2.7 Polymerase Chain Reaction (PCR)

Polymerase Chain Reaction (PCR) is a widely employed molecular technique used to amplify specific DNA sequences through enzymatic activity of a heat-stable DNA polymerase, such as Taq polymerase, in a cyclic thermal process. The reaction mixture typically comprises the target DNA, deoxynucleotide triphosphates (dNTPs), and short oligonucleotide primers complementary to the 3' ends of the target sequences. Amplification occurs in a thermocycler through a three-step cycle. Denaturation at 95°C to separate double stranded DNA, primer annealing at 60°C and extension at 72°C, where the polymerase synthesizes new DNA strands. This cycle is typically repeated 30 or more times to generate a sufficient quantity of the target DNA. Beyond conventional DNA amplification, PCR is also integral to the quantification of nucleic acids such as mRNA and miRNA. In such cases, RNA is first reverse transcribed into complementary DNA (cDNA) using reverse transcriptase. The resulting cDNA can then be quantified through quantitative PCR (qPCR).

2.2.7.1 Reverse Transcription

Reverse transcription is the enzymatic synthesis of cDNA from RNA, catalyzed by reverse transcriptase. The resulting cDNA serves as a template for subsequent PCR amplification.

cDNA was reverse transcribed using SensiFAST™ cDNA synthesis kit, which employs a combination of oligo(dT) and random hexamer primers to enable transcription of a broad range of RNA species. As a starting material, an RNA concentration ranging from 0.3-1.0 µg was used per reaction following the manufacturer's protocol. The details of the reaction mixture composition

and thermocycling conditions are provided in the following tables. The final product was diluted 1:4.5 with 70 µL nuclease free water and stored at -20°C.

Table 9 Reaction mixture for cDNA

Solution	Volume [µL]
5x TransAmp Buffer	4
Reverse transcriptase	1
RNA (0.3-1.0 µg)	n
Nuclease-free water	15-n
Total	20

Table 10 Thermocycler program for reverse transcription

Phase	Temperature	Time
Primer annealing	25 °C	10 min
Reverse transcription	42 °C	15 min
Incubation	48 °C	15 min
Inactivation	85 °C	5 min

2.2.7.2 Quantitative PCR

Quantitative real-time PCR (qPCR) was performed using the SensiMix™ SYBR No-ROX Kit with gene specific primers targeting 13 genes (Table 6). Forward and reverse primers were mixed at equimolar concentrations for each reaction. The qPCR reaction mixture composition and thermocycler program are detailed below.

Table 11 Reaction mixture for qPCR

Solution	Volume [µL]
SensiMix™ SYBR No-ROX	10
Primer F+R	2
cDNA template	5
Nuclease-free water	3
Total	20

Table 12 Thermocycler program qPCR

Phase	Temperature	Time
Initial denaturation	95 °C	10 min
Denaturation	95 °C	15 s
Annealing	61.5 °C	20 s
Extension	72 °C	20 s
Melting curve	60-95 °C	10 min

Amplification was carried out for 45 cycles with an annealing temperature of 61.5°C. Gene expression was normalized against a combination of three housekeeping genes (HKG): RPLP0 (ribosomal protein lateral stalk subunit P0), TBP (TATA-binding protein), and HPRT1 (hypoxanthine phosphoribosyltransferase 1), to minimize technical variability related to sample input, reverse transcription, and PCR efficiency, thereby improving accuracy and cross-run comparability. Despite this approach, batch effects were still evident, as reflected by higher standard deviations in selected targets. Relative quantification of gene expression was performed using the ΔΔCT method implemented in qPCRsoft 4.1, comparing samples to DMSO cultures as baseline control. Expression levels are presented as –ΔΔCT values, reflecting relative gene expression changes without transformation into fold change. Statistical analysis was performed using unpaired t-tests, with Benjamini-Hochberg[85] correction applied to adjust for multiple comparisons across 13 genes and 8 treatment conditions. While several targets (e.g., COL7A1, MMP9) showed raw $p < 0.05$, only TGFB1 under TCN treatment in fibroblast cultures remained significant after correction (Supplementary Table S2). To ensure consistency across qPCR runs, threshold values were manually set to a uniform fluorescence level, and amplification curves were inspected to confirm exponential phase crossing. Amplification consistency and Ct distribution across treatments were visualized in density plots (Supplementary Figure S1 – S2), providing an overview of Ct range and variability in HaCaT and fibroblast cultures. Data validation was supported by qRAT[86] analysis and manual review in Excel, with interpretation focused on consistent trends across treatments.

3. Results

This study investigated the cellular responses of skin epidermis and dermis as 2D models to different treatment conditions relevant to CsA-associated cSCC. The aim was to assess the reproducibility of treatment effects previously observed in 3D OTCs within simplified 2D systems. This approach enabled clearer interpretation of treatment-specific-responses, particularly in gene expression, by minimizing confounding factors arising from co-cultures interactions. HaCaT keratinocytes as epidermis and dermal fibroblasts as the main dermis component, were maintained in cell-specific media and exhibited characteristic morphologies in monolayer culture. Initial investigation focused on the cellular responses to CsA, TCN treatment, UVB exposure, and combinations. CsA has been previously reported to promote mTORC1 activation by stabilizing phosphorylated Akt1, a key regulator of cell survival and proliferation. TCN, as a selective Akt inhibitor, impairs Akt activation by preventing its translocation to the plasma membrane and subsequent phosphorylation by 3-phosphoinositide-dependent kinase 1 (PDK1)[38,87]. By utilizing TCN, this study aimed to isolate and evaluate CsA's downstream effects on mTOR signaling independently of Akt activation. Furthermore, as the main risk factor of skin cancer, UVB radiation was introduced alone and in combination with CsA and TCN to evaluate gene expression and cellular response relevant to skin cancer.

Based on the reported therapeutic blood concentrations of CsA in organ transplant recipients, ranging from approximately 25 to 1250 ng/mL, a working concentration of 1µM was selected for this study[38,88,89]. This dose was applied uniformly to both HaCaT keratinocytes and dermal fibroblasts to assess short-term cellular responses under controlled 2D culture conditions.

Cells were subjected to the following treatment workflow across eight experimental conditions. Cultures treated with CsA were seeded at a higher density to account for potential cytotoxic effects associated with the treatment series:

Table 13 Experimental design

No.	Seeding Cell No.	Day 1 Start	Day 2 Treatment	Day 3 Treatment	Day 4 Harvest
1	400.000	DMSO	-	-	-
2	400.000	DMSO	-	+ UVB (250 J/m^2)	-

3	400.000	DMSO	+ TCN [1 µM]	-	-
4	400.000	DMSO	+ TCN [1 µM]	+ UVB (250 J/m^2)	-
5	600.000	CsA [1 µM]	-	-	-
6	600.000	CsA [1 µM]	-	+ UVB (250 J/m^2)	-
7	600.000	CsA [1 µM]	+ TCN [1 µM]	-	-
8	600.000	CsA [1 µM]	+ TCN [1 µM]	+ UVB (250 J/m^2)	-

3.1 Gene expression analysis in HaCaT following treatments

To investigate the molecular responses of HaCaT keratinocytes to calcineurin inhibitor and stress-related stimuli, gene expression profiling was performed following sequential treatments with CsA, TCN, and UVB irradiation. Since CsA was dissolved in DMSO, cells cultured with DMSO alone served as baseline control. The analysis focused on key signaling pathways and gene categories, including stress-responsive factors (AKT1, NFATc1, ATF3), EMT markers (CDH1, CDH2, ZEB1), TGF-β signaling pathway (TGFB1, SMAD2, SMAD3, SMAD4), and ECM remodeling genes (MMP2, MMP9, COL7A1). This approach would enable the assessment of cellular phenotype, signaling dynamics, and migration related transcriptional changes under various treatment conditions.

3.1.1 Transcriptional response of stress-related genes

This subsection describes the changes in expression levels of AKT1, NFATc1, and ATF3, which are gene regulators in cellular stress responses. Their transcriptional modulation following treatment provides insight into how HaCaT cells adapt to stress stimuli such as CsA, TCN, and UVB.

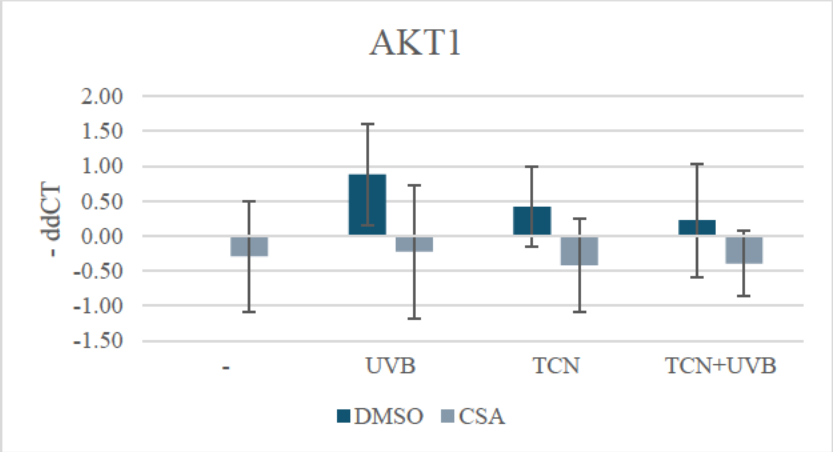

Figure 7: Relative expression of AKT1 in HaCaT cultures. Data represents mean normalized expression levels (-ddCT) relative to DMSO cultures as baseline control (n=3), highlighting treatment-dependent modulation of AKT1 transcription. The modest transcriptional shifts suggest that AKT1 regulation in HaCaT cells may occur primarily through post-translational mechanisms rather than gene-level modulation.

AKT1 expression showed minimal variation across all treatment conditions (Figure 7). A modest increase was observed in the control group following UVB exposure (0.88±0.73), indicating a mild transcriptional response to UVB-induced stress, while other treatments resulted in minimal changes. However, the change was not significant in cells treated with CsA, TCN, or all three stressors, suggesting that these treatments interfered with the normal regulatory responses. Specifically, CsA treatment resulted in a general suppression of AKT1 expression compared to the baseline control, while TCN only and TCN+UVB treatments also blunted by the UVB-driven increase. Overall, these findings suggest that AKT1 transcriptional regulation in HaCaT cells is only mildly responsive to UVB and that CsA and TCN might attenuate this response.

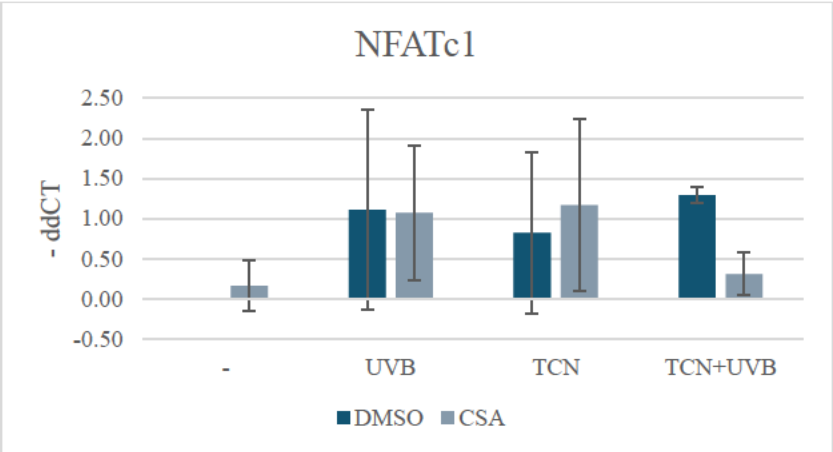

Figure 8: Relative expression of NFATc1 in HaCaT cultures. The gene was strongly induced by UVB and TCN, alone or combined without CsA, reflecting its calcineurin-dependent regulation and its sensitivity to UVB-induced stress (n=3).

NFATc1 gene expression was strongly upregulated in response to UVB, TCN, and combined stimuli in the control groups, indicating a robust transcriptional response to these stimuli (Figure 8). Similarly, CsA-treated cells also showed elevated NFATc1 levels following UVB and TCN treatment. However, under the combined stimuli (CsA+TCN+UVB), NFATc1 expression did not show a significant increase compared to the TCN+UVB control, suggesting that CsA may attenuate NFATc1 transcription. This pattern might support the interpretation that while UVB and TCN act as potent inducers of NFATc1 transcription, CsA might interfere with this response, likely through inhibition of calcineurin-dependent transcriptional activity.

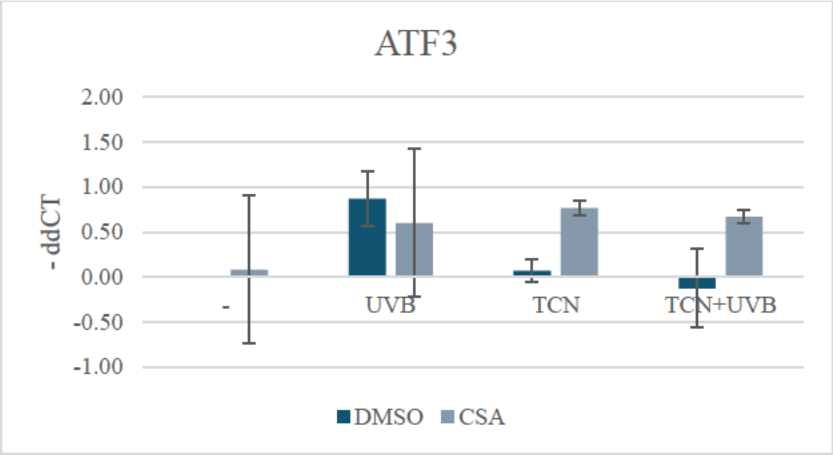

Figure 9:Relative expression of ATF3 in HaCaT cultures. Notable upregulation of ATF3 in response to UVB in control group, while CsA-treated samples exhibited elevated ATF3 levels across conditions (n=3).

ATF3 expression was notably induced by UVB independent of CsA (Figure 9). UVB alone led to increased expression level (0.87±0.3), while TCN alone and both combinations with UVB had only minimal effects. In contrast, CsA alone did not significantly alter ATF3 expression. However, in combination with UVB, TCN, or both, CsA appeared to enhance ATF3 transcription. These findings suggest that while UVB is a primary inducer of ATF3, CsA may amplify this stress-induced transcriptional response under specific conditions. TCN alone was insufficient to induce ATF3, but its combination with CsA resulted in elevated expression, pointing to a complex regulatory mechanism in which CsA modulates the cellular stress response, potentially through pathways involving NFATc1, which has been reported to repress ATF3 transcription.

In general, stress related genes exhibited distinct transcriptional responses to the treatments. AKT1 remained relatively stable, with only mild response following UVB exposure. In contrast, NFATc1 transcription was upregulated under multiple conditions involving UVB and TCN, particularly

when combined with CsA. CsA alone did not alter the expression of any of the three genes, whereas UVB consistently induced transcriptional activation across all targets.

3.1.2 Transcriptional response of EMT related genes

The expression levels of EMT-associated genes, including CDH1, CDH2, and ZEB1, were assessed following treatment to characterize HaCaT responses to different stimuli.

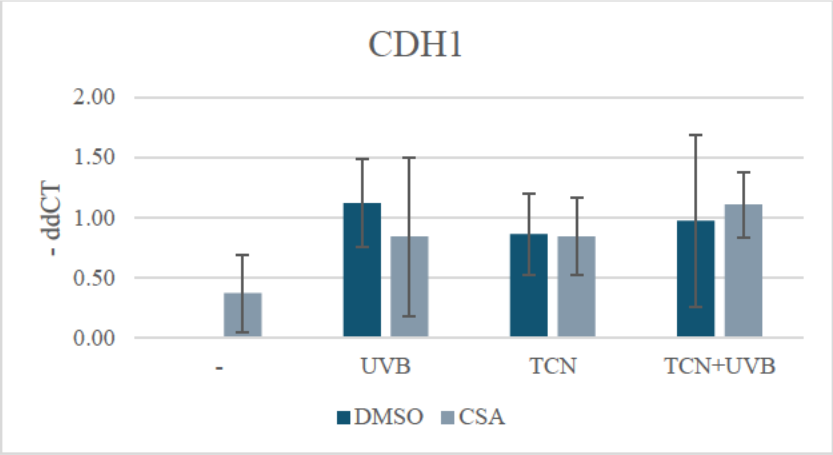

Figure 10:Relative expression of CDH1 in HaCaT cultures. Increased levels were observed across all treatments even under combined stimuli, while CsA alone had only minimal effect (n=3).

The epithelial marker CDH1 was upregulated under all stress conditions, with the most notable increase observed under CsA+TCN+UVB and UVB stimuli in control group, while the treatment with CsA alone caused only minimal change (Figure 10). This pattern suggests that the elevated CDH1 expression may reflect enhanced structural integrity, reduced migratory potential, and preservation of epithelial organization. Interestingly, this upregulation contrasts with the baseline expression, indicating that stress conditions may reinforce epithelial characteristics rather than compromise them.

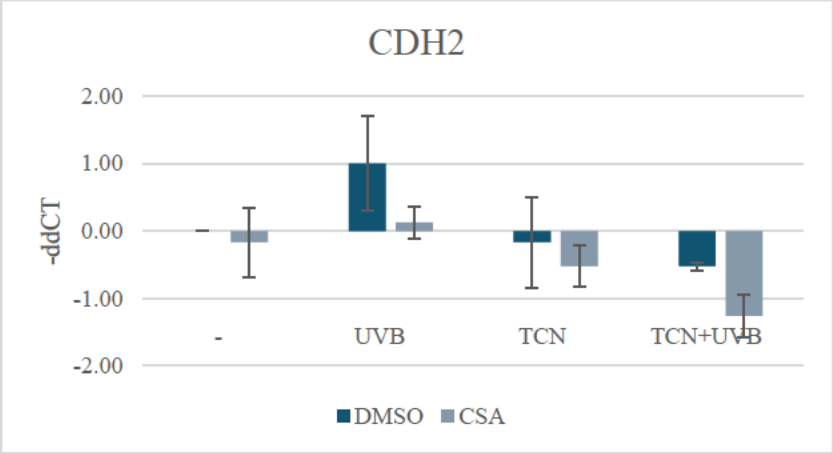

Figure 11: Relative expression of CDH2 in HaCaT cultures. The expression levels varied across conditions, with UVB alone promoting expression level of N-cadherin, while other stimuli led to suppression (n=3).

In contrast to CDH1, CDH2 expression showed a divergent response (Figure 11). UVB alone led to an increase in CDH2 expression, suggesting a stress-induced mesenchymal shift. CsA appeared to abolish this UVB-induced upregulation (decreased value from 1.00±0.71 to 0.13±0.24), indicating a potential suppressive effect of CsA on mesenchymal marker expression. Treatment with TCN or TCN+UVB resulted in downregulation of CDH2, a trend that appeared to be further enhanced by CsA. These findings suggest that CsA may counteract EMT progression by attenuating CDH2 expression, thereby limiting mesenchymal transition under stress conditions.

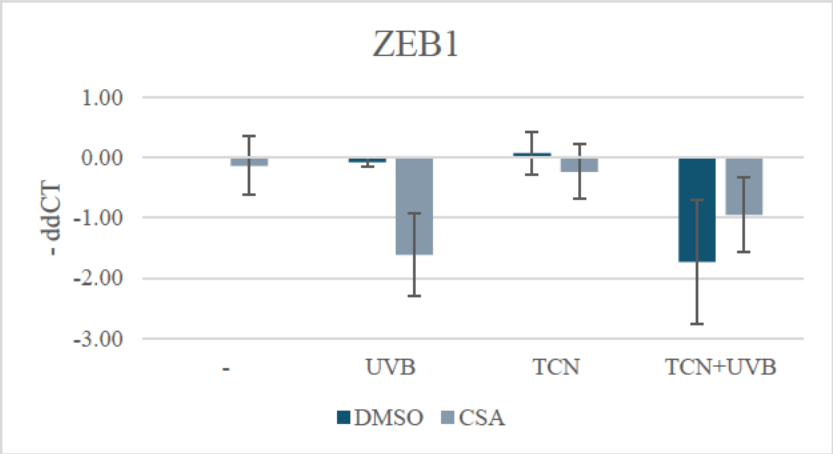

Figure 12: Relative expression of ZEB1 in HaCaT cultures. Slight reduction was observed across treatments, particularly upon CsA+UVB and combined exposure, indicating limited transcriptional activation of ZEB1. The Ct-values were consistently amplified beyond 32 cycles (supplementary section), further suggesting low expression level (n=3).

ZEB1, a key EMT-inducing transcription factor, remained unchanged or downregulated across all treatment conditions (Figure 12). Notably, UVB alone did not significantly reduce ZEB1

expression, whereas treatment with CsA following UVB exposure led to a clear downregulation (-1.61±0.69), suggesting that CsA may actively suppress EMT-related transcriptional activity under stress. Interestingly, TCN+UVB and CsA+UVB treatments showed comparable levels of ZEB1 downregulation, although the presence of CsA appeared to slightly attenuate the suppressive effect observed with TCN+UVB alone. These patterns indicate that CsA modulatory effect may vary depending on the co-administered agents and stress context.

To assess treatment effect on the EMT status, an EMT score was calculated as the ratio of CDH2 to CDH1 expression, based on normalized fold changes derived from ΔΔCT values (Table 14 and Table 15). A higher score indicates a shift toward a mesenchymal phenotype, while a lower score reflects maintenance of epithelial characteristics. Despite CsA's known role in promoting cell migration and invasion, the EMT score progressively decreased across treatments with CsA, CsA+UVB, CsA+TCN, and CsA+TCN+UVB (Figure 13). In comparison, HaCaT cultured in DMSO also showed a downward trend in EMT scores, with the lowest score observed under TCN+UVB (0.36), indicating that both CsA and control groups similarly favored epithelial characteristics. This consistent downward trend does not support EMT induction but rather suggests that HaCaT in 2D cultures retain an epithelial phenotype under conditions that typically promote EMT induction.

Table 14 EMT score analysis in HaCaT cells treated with CsA under various treatment conditions

Gene	Treatment	-ΔΔCT	Norm.expression ($2^{-\Delta\Delta CT}$)	EMT score (CDH2/CDH1)
CDH2	CsA	-0.17	0.90	0.69
CDH1		0.37	1.31	
CDH2	CsA+UVB	0.13	1.14	0.61
CDH1		0.84	1.86	
CDH2	CsA+TCN	-0.52	0.69	0.39
CDH1		0.84	1.78	
CDH2	CsA+TCN+UVB	-1.26	0.42	0.20
CDH1		1.11	2.15	

Table 15 EMT score analysis in HaCaT cells in control group under various treatment conditions

Gene	Treatment	-ΔΔCT	Norm.expression ($2^{-\Delta\Delta CT}$)	EMT score (CDH2/CDH1)
CDH2	-	0.00	1.00	1.00
CDH1		0.00	1.00	
CDH2	UVB	1.00	2.00	0.92
CDH1		1.12	2.17	
CDH2	TCN	-0.17	0.89	0.49

CDH1		0.86	1.82	
CDH2	TCN+UVB	-0.52	0.70	0.36
CDH1		0.97	1.96	

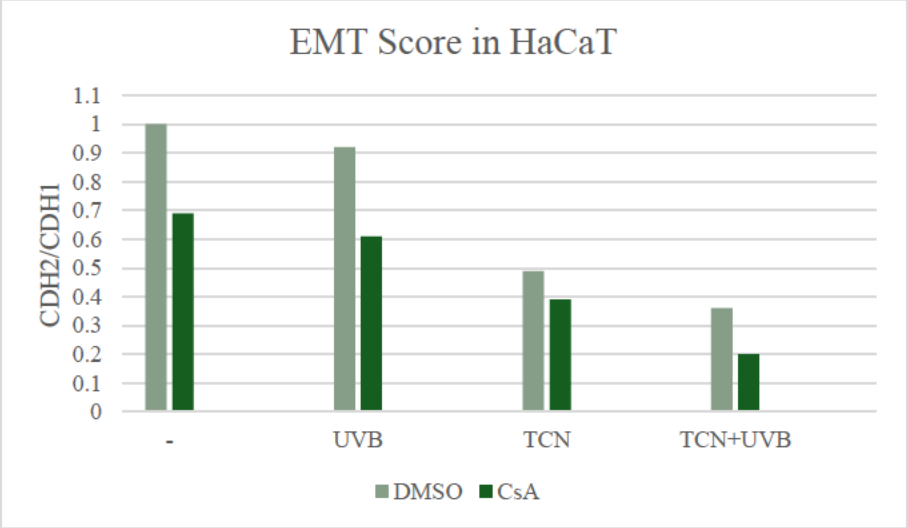

Figure 13: EMT score across controls and CsA-based treatments in HaCaT. The graph shows a progressive decrease in EMT score following exposure to stress factors, indicating a shift away from mesenchymal features and toward a more epithelial phenotype. EMT scores were calculated based on the relative expression of CDH1 and CDH2 markers.

Overall, the findings in gene expression were evaluated in relation to the EMT process. A shift toward EMT was initially expected for treatments involving CsA. Interestingly, contrary to the expectation, transcription of epithelial marker (CDH1) was increased across all conditions. Whereas mesenchymal marker (CDH2) level increased only following UVB exposure, while remaining unchanged or downregulated under other conditions. Additionally, none of the treatments led to an upregulation of ZEB1. These results, together with the observed reduction in EMT scores, support the maintenance of an epithelial phenotype following treatment.

3.1.3 Transcriptional response of TGF-β signaling pathway related genes

In the following subsection the expressions of SMAD2, SMAD3, SMAD4, and TGFB1 were measured following treatment, reflecting TGF-β pathway involvement in HaCaT cell responses.

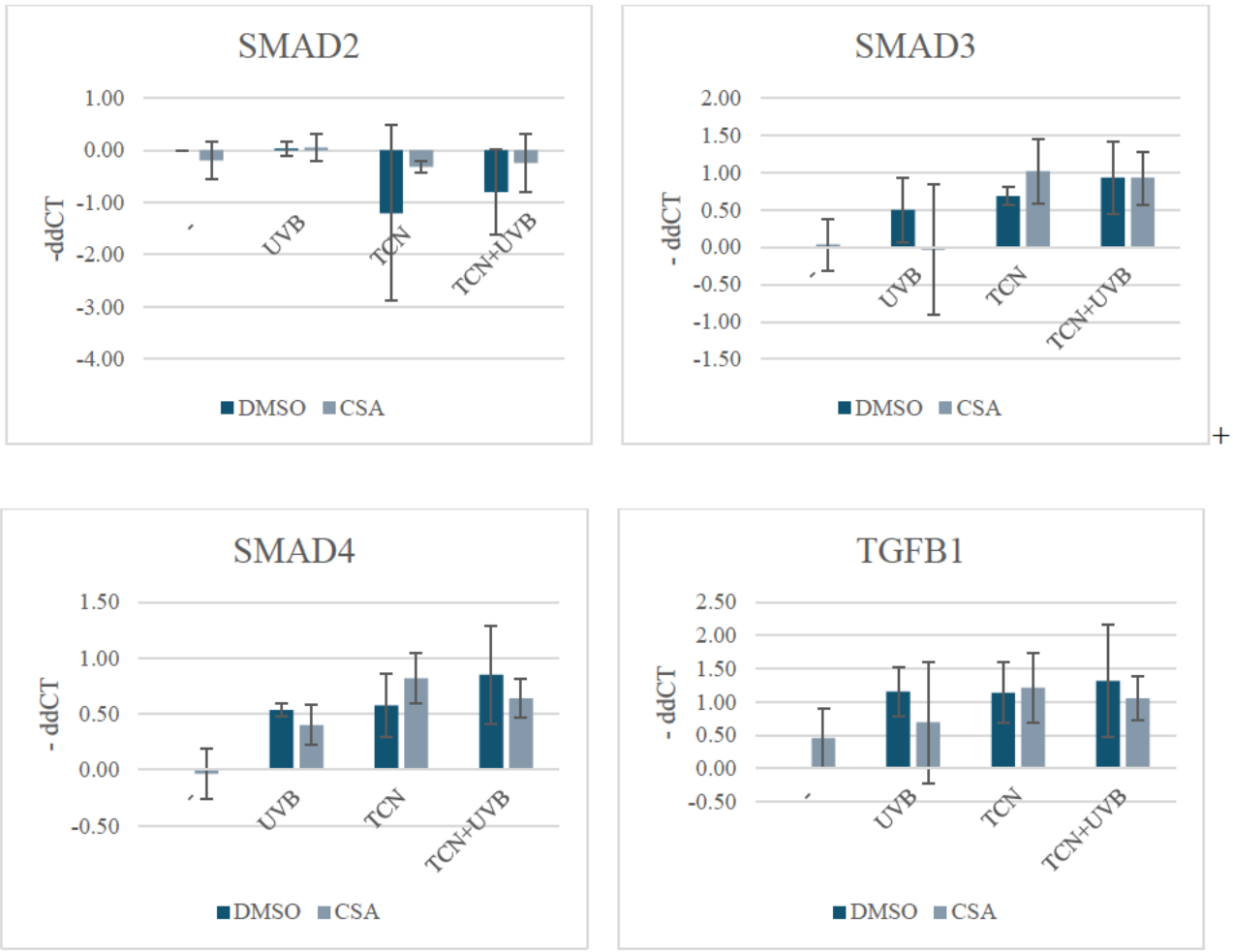

Figure 14: Relative expressions of SMAD2, SMAD3, SMAD4, and TGFB1 in HaCaT cultures. TCN treatment combined with CsA led to a coordinated upregulation of TGFB1 and SMAD3/4, with SMAD3 exhibiting the most pronounced increase among the SMADs family. In contrast, UVB or CsA alone had limited effect on gene expression (n=3).

Gene expression analysis revealed rather consistent upregulation of SMAD3, SMAD4, and TGFB1 in response to all treatments, with SMAD3 under CsA+UVB as exception (Figure 14). This pattern indicates partial activation of the canonical TGF-β/SMAD signaling pathway (Figure 5). The increase in TGFB1 expression was particularly robust, suggesting a strong transcriptional response to stress. In contrast, SMAD2 expression remained unchanged or downregulated, especially under TCN and TCN+UVB treatments, pointing to selective modulation within the TGF-β pathway. These findings imply that while TGFB1 is transcriptionally responsive to UVB, TCN and both combinations, a full engagement of downstream SMAD signaling might be limited under the current experimental conditions.

Overall, the transcriptional upregulation of TGFB1, SMAD3, SMAD4 across most treatments suggest partial activation, with TGFB1 showing strongest response. The lack of consistent

SMAD2 regulation, particularly under TCN-related conditions, points to selective pathway engagement rather than full activation.

3.1.4 Transcriptional response of ECM remodeling related genes

The expression levels of ECM-related genes, including COL7A1, MMP2, and MMP9, were assessed following treatments to evaluate changes in matrix remodeling and epithelial integrity in HaCaT cells.

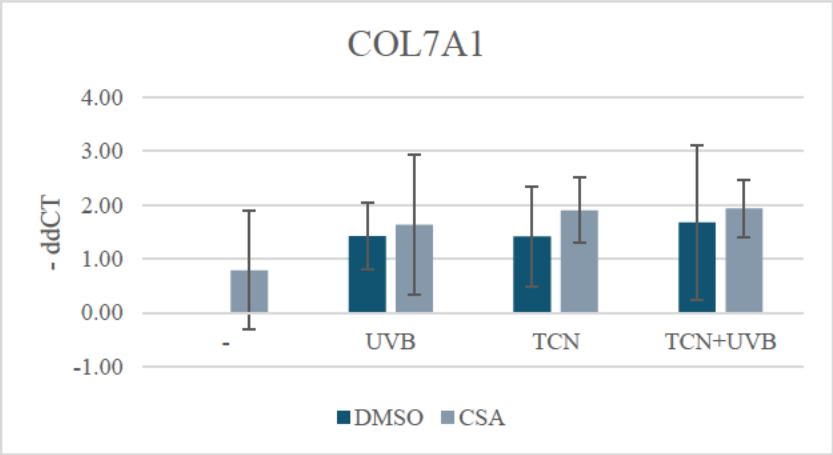

Figure 15: Relative expression of COL7A1 in HaCaT cultures. COL7A1 expression was consistently upregulated, with the highest levels under combined stress treatments, reflecting a robust repair response (n=3).

COL7A1 expression was consistently upregulated across all treatment conditions, while CsA alone showed only minimal effect with 0.79±1.10 (Figure 15). The presence of CsA seemed to further increase the transcription. Though smaller compared to CsA treatments, control groups also showed increased expression, suggesting a robust response to stress aimed at reinforcing epithelial integrity following UVB-induced damage and kinase inhibition.

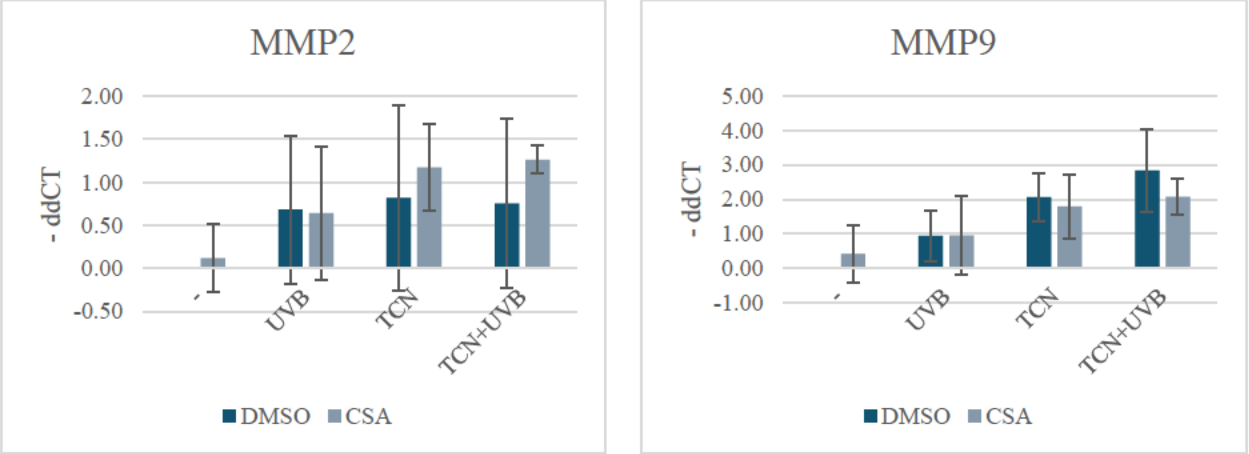

Figure 16: Relative expressions of MMP2 and MMP9 in HaCaT cultures. MMP2 showed moderate upregulation under stress while MMP9 displayed a pronounced, condition-dependent increase, peaking under all stress factors. CsA appeared to reduce MMP9 induction (n=3).

MMP2 expressions were moderately upregulated across all treatments (Figure 16). Under the presence of CsA, the TCN and combined TCN+UVB cultures showed further increase in transcription (1.17 to 1.26, respectively). Control group also showed increased expression ranging from ~0.68 to ~0.82, though to a lesser extent compared to CsA treatment, suggesting a general activation of MMP2 under stress conditions. In the other hand, MMP9 showed a more pronounced and condition-dependent increase, with the highest induction observed after TCN+UVB treatment (2.83±1.21). The higher induction of MMP after combined treatment, compared to the sum of individual treatments, might indicate a potential synergistic effect of TCN and UVB on MMP9 transcription in the absence of CsA.

Together, these observations highlight differential regulation of ECM-related genes, with COL7A1 consistently elevated, MMP2 modestly increased by combined treatments, and MMP9 showing a strong, condition-specific increase, particularly under TCN+UVB. All ECM remodeling genes analyzed above were positively regulated following treatment, despite their differing roles in ECM dynamics. While CsA alone induced only minor changes, the other treatments resulted in a more pronounced transcriptional increase, especially for MMP9.

3.2 CsA-induced modulation of HaCaT cell migration

To investigate the impact of CsA on epithelial cell behavior, a migration (scratch) assay was performed. Given CsA's known influence on signaling pathways such as PI3K/Akt[38] and its potential to induce EMT-like features, this assay aimed to quantify changes in migratory capacity

following different treatments in a 2D culture over a 24-hour period following a scratch. Cells cultured in DMSO served as vehicle control alongside CsA. Mitomycin C (MMC) was used to inhibit cell proliferation, isolating the effects to migration rather than cell growth. Following MMC incubation, cultures were returned to normal growth medium containing DMSO or CsA, with or without TCN (method section 2.2.4).

Additionally, UVB irradiation as the main risk factor for skin cancer was included to simulate environmental stress and assess potential synergistic effects with CsA. The combination of pharmacological and environmental stimuli would provide insight into how keratinocyte migration is modulated under conditions relevant to skin carcinogenesis in immunosuppressed individuals. The results presented below illustrate the temporal dynamics of gap closure and highlight differential responses to CsA, TCN, and UVB following short-term exposure.

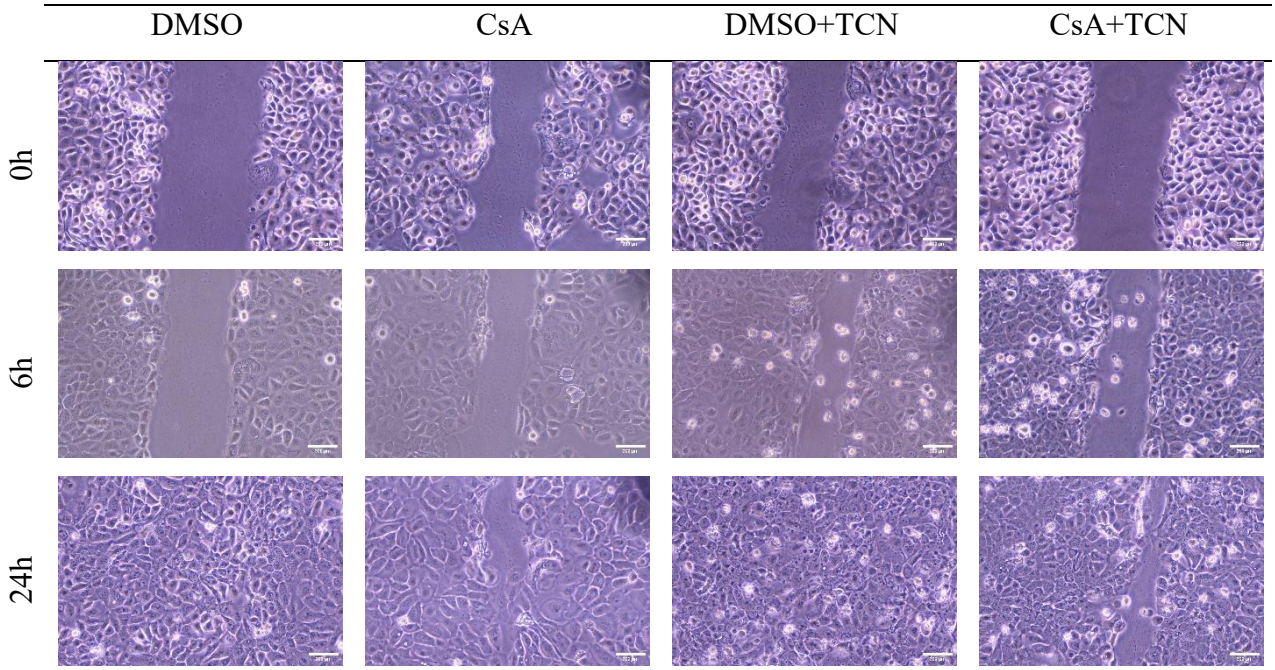

Figure 17: Time-course analysis of HaCaT cell migratory behavior under different treatment conditions. Representative images of monolayer cultures at 0-,6-, and 24-hours post-scratch, containing DMSO (control), CsA, and TCN. The images illustrate treatment-dependent differences in gap closure over time. Scale bar represents 300µm.

After 24 hours, HaCaT cells cultured in DMSO exhibited complete gap closure, indicating robust migratory capacity under baseline conditions. In contrast, CsA culture displayed a persistent gap at 24 hours, with slightly reduced migration compared to baseline (Figure 17). Interestingly, despite TCN's known cytotoxicity and inhibitory effect on Akt signaling[38], TCN culture also showed substantial gap closure, suggesting that short-term exposure at the applied concentration

did not significantly impair migration in HaCaT cells. The most pronounced migration inhibition was observed in CsA+TCN culture, where the gap remained open after 24 hours. This points to a synergistic or additive inhibitory effect of CsA and TCN on HaCaT migration, likely due to disruption of CsA-mediated Akt signaling (Figure 7).

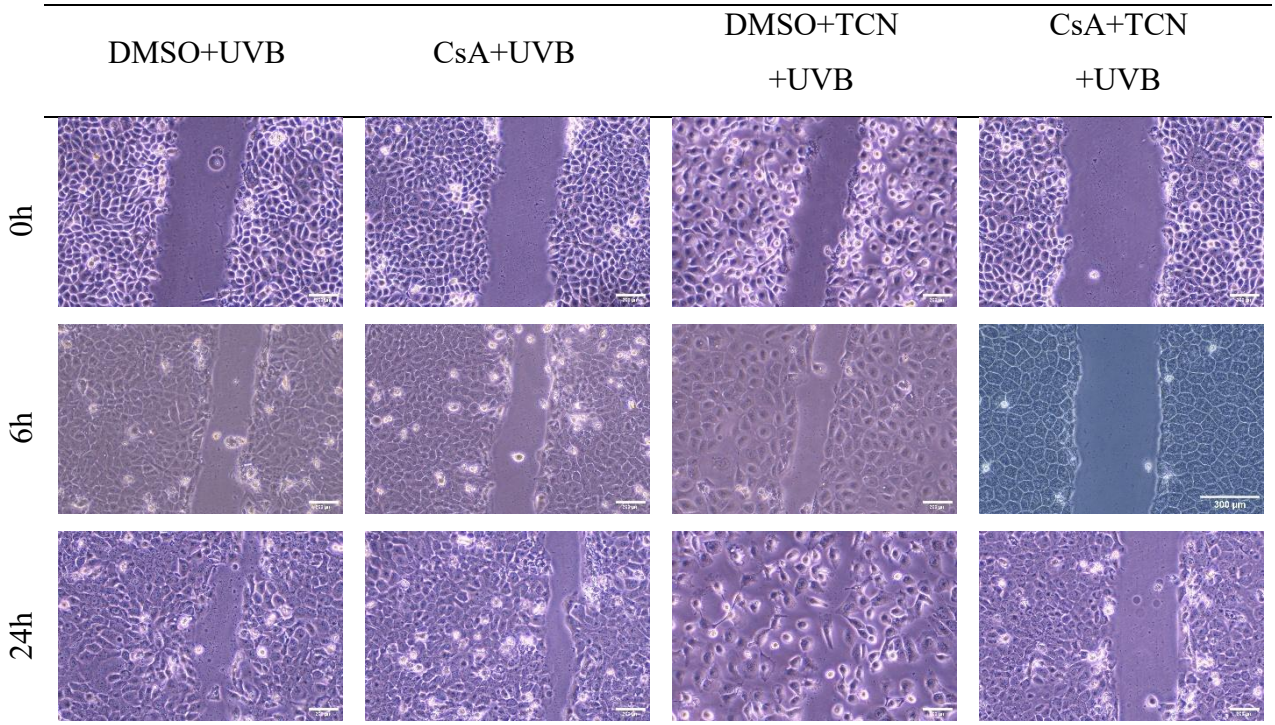

Figure 18: Time-course analysis of HaCaT cell migratory behavior under combined UVB and pharmacological treatments. Representative images of monolayer cultures at 0-,6-, and 24-hours post-scratch. The images illustrate treatment-dependent differences in gap closure over time. The 6-hour image for the CsA+TCN+UVB culture was captured in PBS due to excessive debris in the medium. Scale bar represents 300µm.

Following UVB irradiation, cell migration was further assessed in all experimental groups (Figure 18). After 6 hours, UVB induced visible stress responses across all conditions, as evidenced by the presence of cell debris, with culture under TCN+UVB as exception. This may reflect early apoptotic signaling, potentially mediated by UVB-induced NFAT activation[90]. The extent of cellular disruption, specifically the formation of cell debris following UVB irradiation, was assessed qualitatively through morphological observations rather than quantified using a defined analytical method. Although the debris was not sharply defined, the presence of floating white dots supports qualitative observations of UVB-induced cellular stress. The most severe disruption was observed in the CsA+TCN+UVB condition, where the extensive debris was noted, suggesting compounded cytotoxicity from the combined treatments. The 6-hour image for this culture was acquired in PBS to improve visualization due to excessive debris in the CsA-containing medium.

Nevertheless, despite the change in imaging medium, substantial debris remained evident, further underscoring the extent of cellular damage (Supplementary Figure S3).

At 24 hours, cultures exposed to UVB in both groups showed similar partial gap closure, compared to non-irradiated controls (Figure 18 to Figure 17). This indicates that while UVB impairs migration[91] and damage[92] of the keratinocytes, HaCaT cells still retain limited migratory potential under these conditions. Moreover, treatment with CsA+UVB resulted in similar partial gap closure to UVB alone. This incomplete closure may indicate that CsA, in combination with UVB, does not promote migration beyond UVB alone.

In contrast, DMSO+TCN+UVB culture exhibited partial monolayer disruption, with widespread cell detachment after 24 hours. The disrupted monolayer integrity points to exacerbated cellular damage when both UVB and TCN are present, even without CsA. Additionally, CsA+TCN+UVB culture, despite showing substantial debris at 6 hours, retained monolayer integrity at 24 hours, with cells remaining adherent and the scratch clearly open.

This observation revealed that while HaCaT cells retained baseline motility under DMSO and short-term TCN exposure, CsA and its combination with TCN impaired gap closure. UVB irradiation further reduced migration and induced cell stress. Monolayer integrity was partially preserved during the treatment, suggesting complex interactions between calcineurin inhibitor and cytotoxic stressors affecting keratinocytes migration and survival.

3.3 Gene expression analysis in fibroblasts following treatments

To investigate the transcriptional responses of fibroblasts to stress inducing treatments, gene expression profiling was conducted following sequential exposure to CsA, TCN, and UVB irradiation. Cells cultured in DMSO served as reference control. The analysis focused on key regulatory pathways including stress responsive transcription factors, TGF-β/SMAD signaling, and ECM remodeling. Given the inherently mesenchymal nature of fibroblasts, EMT markers were evaluated to assess shifts in phenotypic plasticity and activation rather than transition. This approach would enable a comprehensive assessment of CsA's impact on fibroblast behavior under various stress conditions.

3.3.1 Transcriptional response of stress-related genes

This subsection describes the changes in expression levels of AKT1, NFATc1, and ATF3, which are gene regulators in cellular stress responses. Their transcriptional modulation following treatment provides insight into how fibroblast cells adapt to environmental stressors such as CsA, TCN, and UVB.

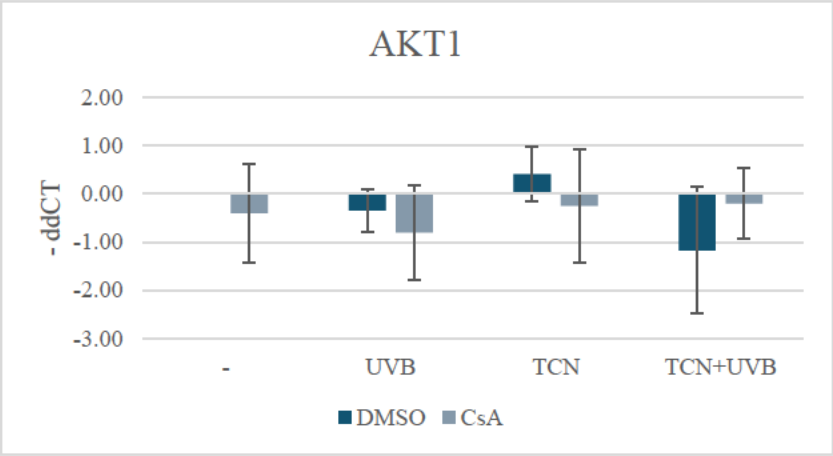

Figure 19: Relative expression of AKT1 in fibroblast cultures. TCN alone slightly increased AKT level, while UVB and TCN+UVB downregulated it. CsA consistently reduced AKT1 levels across all stress conditions (n=3).

AKT1 expression showed variable responses across treatment conditions (Figure 19). The most pronounced change was observed following TCN+UVB treatment (-1.17±1.31). In contrast, single treatments with UVB or TCN alone caused only minor and opposing effects. Interestingly, the strong reduction in AKT1 transcription induced by TCN+UVB was attenuated by CsA, suggesting a potential antagonistic role of CsA. Furthermore, treatment with CsA+UVB also led to a slight decrease in AKT1 expression.

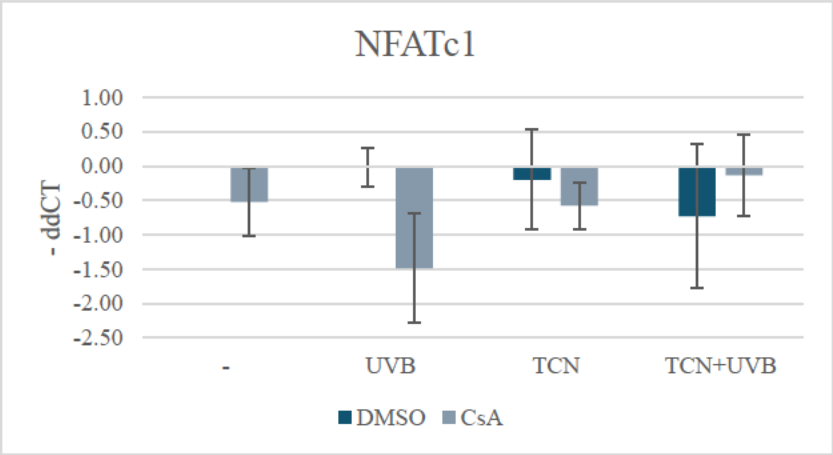

Figure 20: Relative expression of NFATc1 in fibroblast cultures. Expression was broadly downregulated, with strongest suppression in CsA+UVB. These findings suggest inhibition of calcineurin-NFAT signaling and UVB-induced transcriptional repression (n=3).

NFATc1 was generally downregulated across all treatments (Figure 20). The most notable reduction occurred in CsA+UVB (-1.48±0.8), whereas the single treatment with UVB or CsA alone caused only a minor change (-0.02 and -0.52, respectively). These results are consistent with CsA's known inhibition of calcineurin-NFAT signaling and suggest that UVB may further suppress NFATc1 through stress-induced pathways in fibroblast cultures. The combined effects of CsA and UVB likely contribute to a diminished transcriptional activity of NFATc1 in fibroblasts under stress. A decrease in NFATc1 expression was also detected following TCN+UVB treatment.

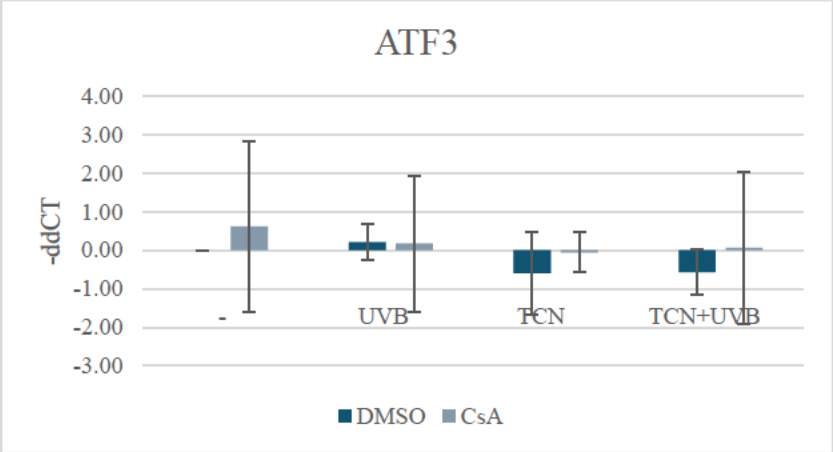

Figure 21: Relative expression of ATF3 in fibroblast cultures. Expression was modestly elevated in CsA-only fibroblasts, while other treatments showed baseline or reduced levels. These findings suggest ATF3 is more responsive to CsA than to UVB or TCN in fibroblasts, possibly due to cell-type specific stress sensitivity (n=3).

ATF3 expression was moderately elevated in CsA-only fibroblasts but remained close to baseline in other conditions (Figure 21). TCN and in combination with UVB led to downregulation in control groups. These findings suggest that ATF3 is not strongly induced by UVB or TCN in fibroblasts, and its expression may be more sensitive to CsA exposure.

In contrast with the HaCaT response, where ATF3 was more strongly UVB-inducible, the expression of ATF3 in fibroblasts was modestly increased in CsA only treatment. This finding suggests that fibroblasts may be less transcriptionally responsive to UVB or kinase inhibition via ATF3 under the tested conditions.

The selective activation of AKT1, NFATc1, and ATF3 in fibroblasts underscores a more controlled stress response, emphasizing the importance of cell-type-specific dynamics in interpreting stress-induced transcriptional changes.

3.3.2 Transcriptional response of EMT related genes

The expression levels of EMT-associated genes, including CDH1, CDH2, and ZEB1, were assessed following treatment to characterize fibroblast responses to different stimuli.

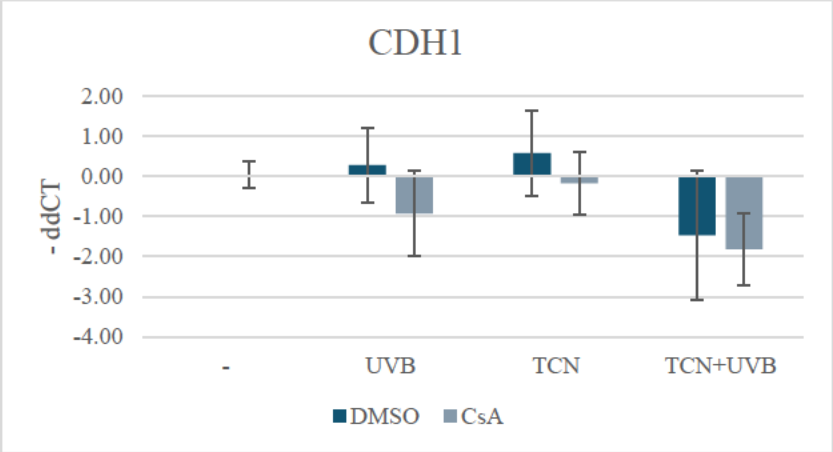

Figure 22: Relative expression of CDH1 in fibroblast cultures. Expression was generally low and variable, with strongest downregulation in TCN+UVB-treated fibroblasts. These findings suggest limited epithelial marker induction under combined stress (n=3).

In fibroblasts, CDH1 level was generally low and variable across conditions, with the most notable downregulation occurred under TCN+UVB treatment in both groups (Figure 22). This indicates that fibroblasts do not significantly upregulate epithelial markers in response to stress, even when exposed to combined pharmacological and/or UVB stimuli. The lack of induction may reflect the inherent mesenchymal phenotype of fibroblasts and their limited plasticity toward epithelial-like transitions under these conditions.

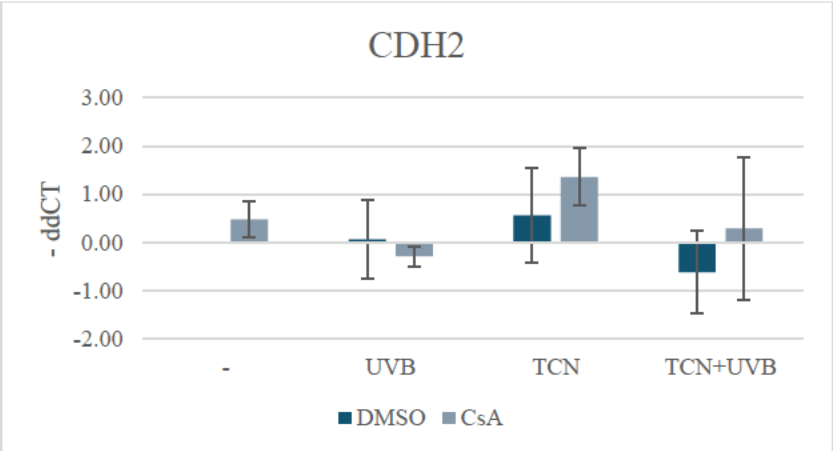

Figure 23: Relative expression of CDH2 in fibroblast cultures. CDH2 was elevated in response to TCN, especially with CsA, while UVB alone had minimal effect. Combined stress led to moderate downregulation in control and no significant effect in CsA culture (n=3).

In contrast, CDH2 expression showed a more dynamic response to treatment compared to CDH1. Exposure to TCN led to increased CDH2 levels, particularly when combined with CsA (1.36±0.59),

while UVB alone had minimal effect (Figure 23). Interestingly, combined stress treatments led to moderate CDH2 downregulation in both groups compared to TCN-treated cultures.

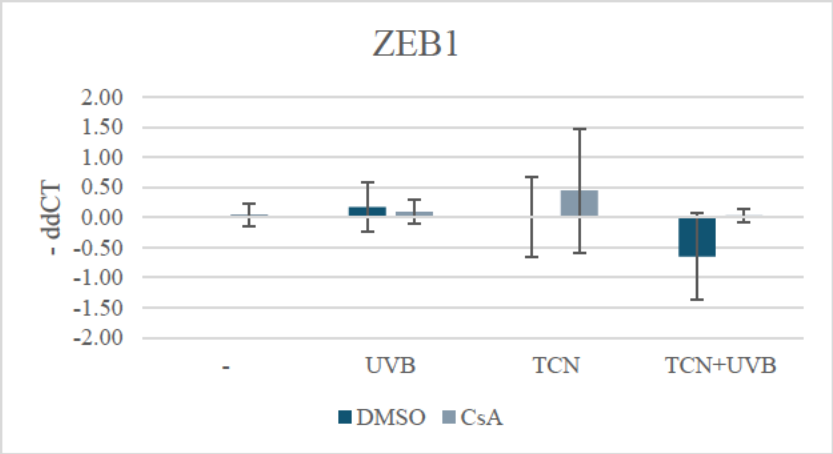

Figure 24: Relative expression of ZEB1 in fibroblast cultures. Expression remained largely stable, with modest upregulation in CsA+TCN. These findings suggest that EMT regulation via ZEB1 was not a dominant transcriptional mechanism under short-term stress (n=3).

ZEB1 levels remained relatively stable across most treatment conditions, with only modest upregulation in CsA+TCN (0.44±1.03) and slight downregulation in TCN+UVB (-0.65±0.73), indicating that ZEB1 expression was not markedly altered by the treatments applied over the short-time period (Figure 24).

The EMT score, calculated as the ratio of CDH2 to CDH1, provides insight into the mesenchymal state of fibroblasts under CsA-based treatments (Table 16). The score progressively increased from 1.36 in CsA alone to 4.32 under triple stress, indicating sustained mesenchymal characteristics with the addition of stressors. In comparison, EMT scores in the DMSO control group remained lower across all conditions, ranging from 0.86 under UVB to 1.80 under TCN+UVB (Table 17), suggesting that CsA may amplify the EMT score in fibroblast.

Table 16 EMT score analysis in fibroblast cells treated with CsA under various treatment conditions

Gene	Treatment	-ΔΔCT	Norm. expression ($2^{-\Delta\Delta Ct}$)	EMT score (CDH2/CDH1)
CDH2	CsA	0.48	1.39	1.36
CDH1		0.04	1.03	
CDH2	CsA+UVB	-0.29	0.82	1.55
CDH1		-0.92	0.53	
CDH2	CsA+TCN	1.36	2.57	2.87
CDH1		-0.16	0.90	
CDH2	CsA+TCN+UVB	0.29	1.22	4.29
CDH1		-1.81	0.29	

Table 17 EMT score analysis in fibroblast cells in control group under various treatment conditions

Gene	Treatment	-ΔΔCT	Norm.expression ($2^{-\Delta\Delta CT}$)	EMT score (CDH2/CDH1)
CDH2	-	0.00	1.00	1.00
CDH1		0.00	1.00	
CDH2	UVB	0.06	1.04	0.86
CDH1		0.28	1.21	
CDH2	TCN	0.56	1.47	0.99
CDH1		0.58	1.49	
CDH2	TCN+UVB	-0.62	0.65	1.80
CDH1		-1.47	0.36	

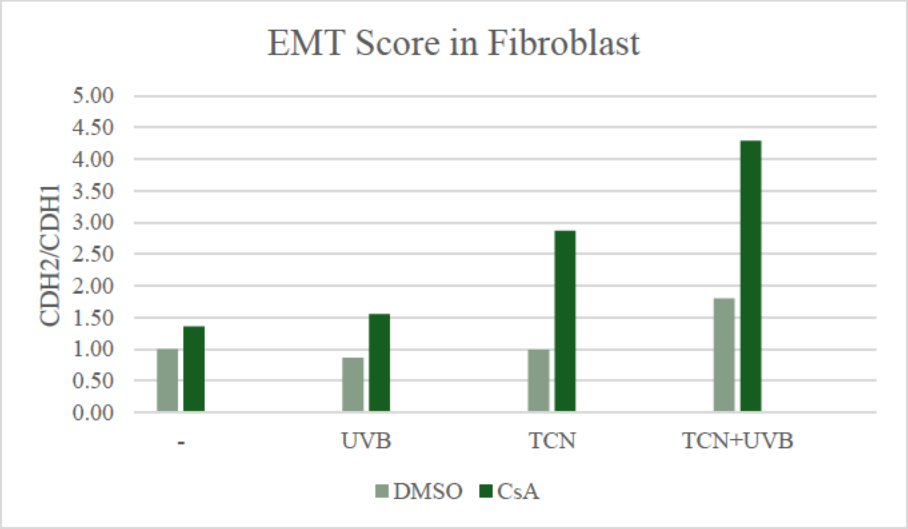

Figure 25: EMT score across control and CsA-based treatments in fibroblasts. The score increased progressively from CsA alone to triple stress. This indicates enhanced mesenchymal characteristics under combined stress, likely reflecting fibroblasts' activation. EMT scores were calculated based on the relative expression of CDH1 and CDH2 markers.

Collectively, the transcriptional response of CDH1, CDH2 and ZEB1 was determined to assess the treatment-induced changes in fibroblast activation and mesenchymal plasticity. A shift toward a more pronounced EMT-like profile was observed in all CsA-containing treatment, with the highest EMT score recorder under CsA+TCN+UVB, suggesting enhanced mesenchymal activation rather than a true transition.

3.3.3 Transcriptional response of TGF-β signaling pathway related genes

In this subsection the expressions of SMAD2, SMAD3, SMAD4, and TGFB1 were measured following treatment, reflecting TGF-β pathway involvement in fibroblast cell responses.

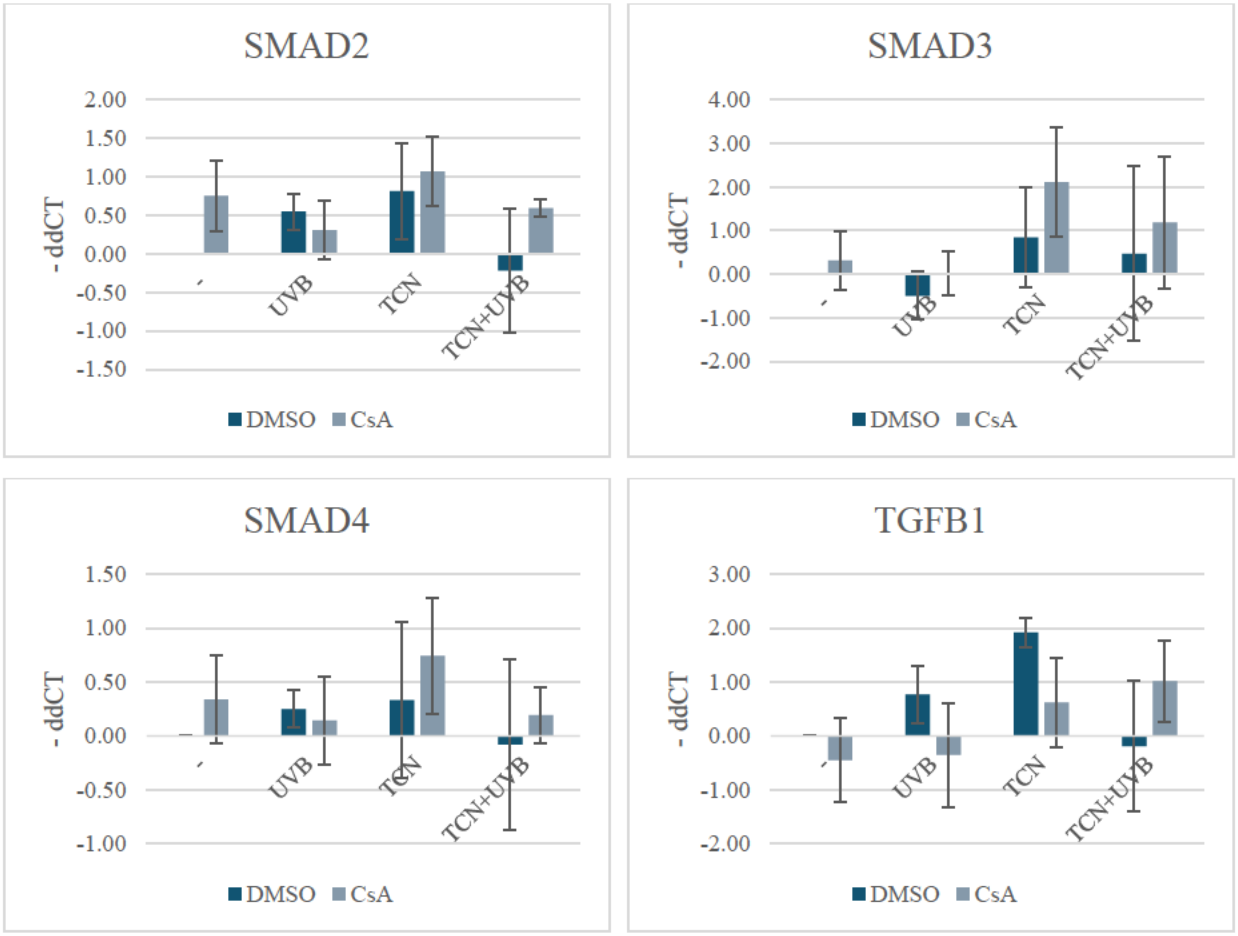

Figure 26: Relative expression of SMAD2, SMAD3, SMAD4, and TGFB1 in fibroblast cultures. TCN treatments, partially with CsA, induced coordinated upregulation of TGFB1 and SMADs, with SMAD3 showing the strongest response. This pattern suggests activation of canonical TGF-β pathway under kinase inhibition, while UVB or CsA alone had minimal impact (n=3).

The expression of SMAD2 was moderately elevated in response to TCN treatment independent of CsA. Increased level of SMAD2 was also found after treatment with CsA, UVB and CsA+TCN+UVB. SMAD3 showed the strongest induction among SMAD family, particularly following CsA+TCN exposure, suggesting a robust transcriptional response. SMAD4 expression was modestly increased in the cultures treated with CsA+TCN but remained unchanged under other conditions. TGFB1 expression was notably increased in UVB, TCN and CsA+TCN+UVB cultures (Figure 26).

Overall, the expression profiles suggest selective activation with TCN treatment eliciting the most consistent transcriptional response, especially in combination with CsA. TCN triggers coordinated upregulation of TGFB1 and SMAD2/3/4, consistent with activation of the canonical TGF-β pathway.

3.3.4 Transcriptional response of ECM remodeling related genes

The expression levels of ECM-related genes, including COL7A1, MMP2, and MMP9, were assessed following treatment to evaluate changes in matrix remodeling and epithelial integrity in fibroblast cells.

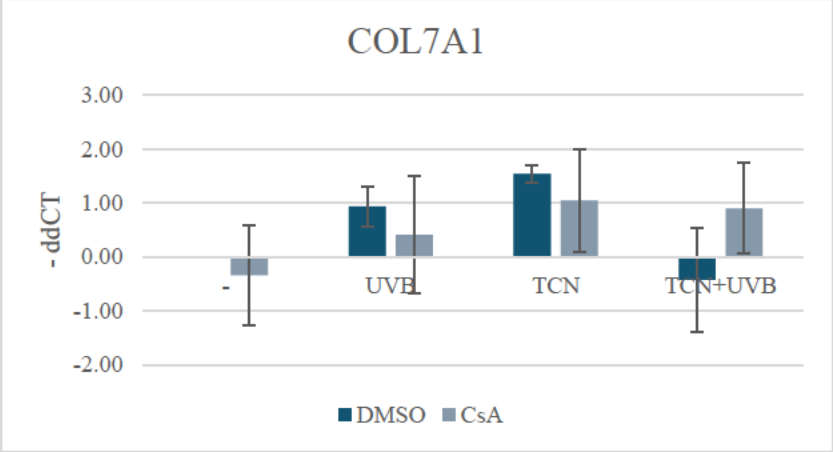

Figure 27: Relative expression of COL7A1 in fibroblast cultures. Expression was strongly upregulated by TCN, especially without the presence of CsA, while UVB induced a moderate increase (n=3).

COL7A1 expression was strongly upregulated in response to TCN, particularly under TCN alone, with a lesser extent of induction observed in the CsA+TCN condition (Figure 27). UVB alone induced a moderate increase in COL7A1 transcription. However, the induction by TCN was suppressed under combined stress conditions, suggesting that co-treatment may dampen matrix production. CsA+TCN+UVB resulted in similar level of COL7A1 expression as observed under UVB alone, indicating that the combined treatment did not further enhance COL7A1 transcription.

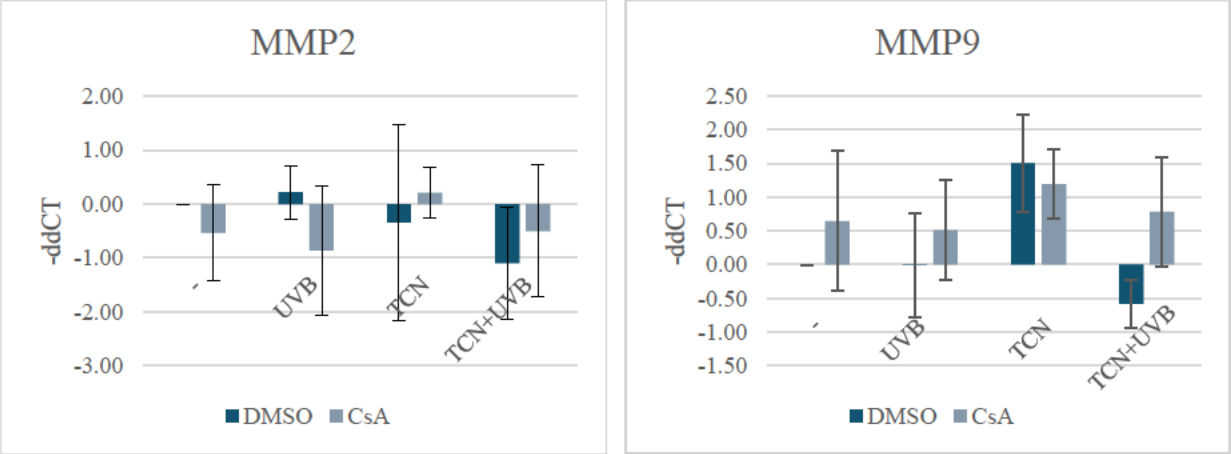

Figure 28: Relative expressions of MMP2 and MMP9 in fibroblast cultures. MMP2 was generally downregulated, while MMP9 was markedly upregulated by TCN, indicating dual ECM remodeling. TCN promotes matrix turnover via MMP9 and matrix preservation via MMP2 suppression (n=3).

MMP2 expressions were generally downregulated across most conditions, whereas MMP9 levels were mostly increased, revealing distinct ECM remodeling responses in fibroblasts under stress conditions (Figure 28). The largest change to MMP2 was detected after TCN+UVB treatment (-1.10±1.05), suggesting suppression of matrix degradation. For MMP9 the highest change was measured in TCN treated fibroblasts in the absence of CsA, indicating enhanced matrix turnover.

Collectively, the observation reveals distinct responses among ECM related genes under stress conditions. The data points out the critical function of TCN in this process, which appears to induce a dual ECM remodeling response in fibroblasts: enhancing matrix production via COL7A1 and promoting matrix turnover through MMP9. This is consistent with the activation of TGF-β signaling observed in earlier results (Figure 26) and may reflect a stress-adaptive or reparative phenotype.

3.4 CsA-induced modulation of fibroblast cell migration

To complement the analysis of epithelial responses, dermal fibroblasts were subjected to the same scratch assay (result section 3.2) to evaluate the treatments on mesenchymal cell migration. Unlike keratinocytes, fibroblasts are inherently migratory and play a central role in extracellular matrix (ECM) remodeling and wound healing process.

This experiment aimed to determine whether CsA alters fibroblast motility and whether UVB exposure further modulates this behavior. Fibroblasts cultured in the medium containing DMSO are the control to each treatment. Given the role of fibroblasts in potentially shaping the TME and

facilitating epithelial invasion[93–95], understanding their response to stress-simulating factors is critical. The following results detail the migration kinetics observed under different treatment conditions.

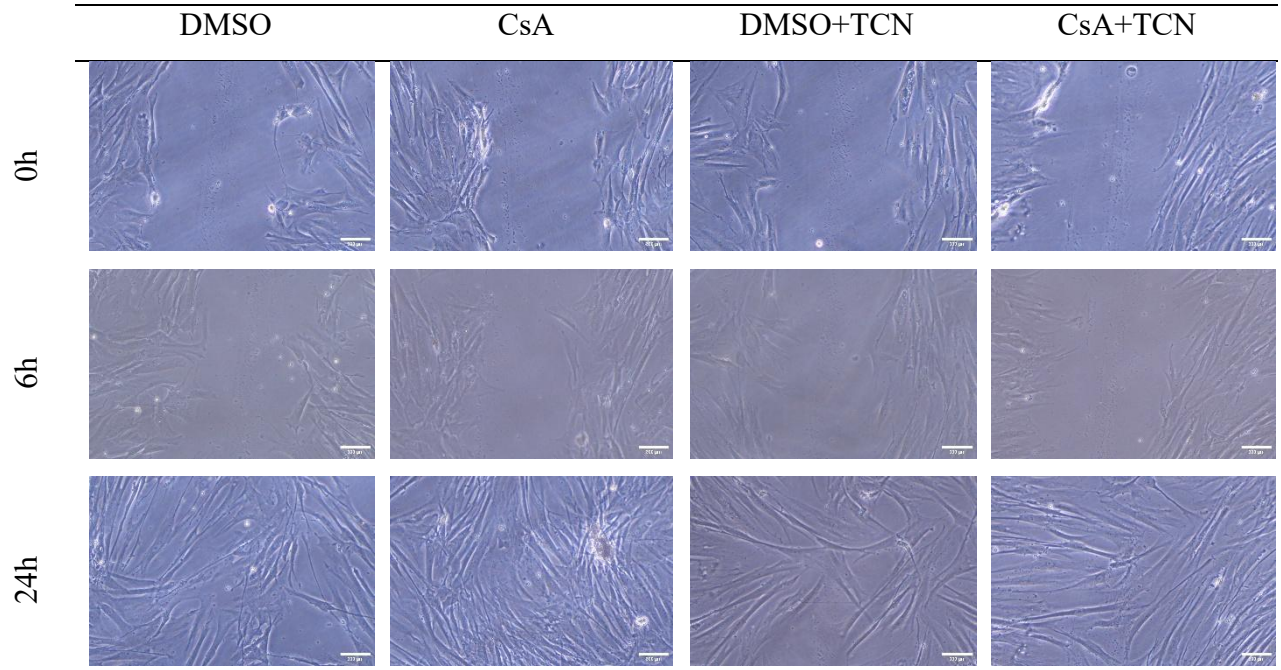

Figure 29: Time-course analysis of fibroblasts cell migratory capacity under different treatment conditions. Representative images of monolayer cultures at 0-, 6-, and 24- hours post-scratch. The images illustrate treatment-dependent differences in gap closure over time. Scale bar represents 300µm.

Fibroblasts cultures in both groups achieved complete gap closure by 24 hours, despite initial slowing observed at 6 hours (Figure 29). This indicates robust migratory capacity and good tolerance to short-term CsA exposure at the applied dose under 2D culture conditions. In contrast, TCN-treated cultures exhibited a slight delay in gap closure, with the scratch still faintly visible at 24 hours (specifically DMSO+TCN). This suggests that TCN modestly impairs fibroblast migration. Given Akt signaling central role in remodeling and motility, its involvement in this migratory response warrants further investigation.

Importantly, monolayer integrity was preserved across all conditions, with no significant cell detachment or debris formation, highlighting fibroblast resilience to short-term CsA and TCN exposure. Higher seeding densities might have further supported gap closure, particularly in CsA-treated cultures, where more crowded cells could fill the scratch area.

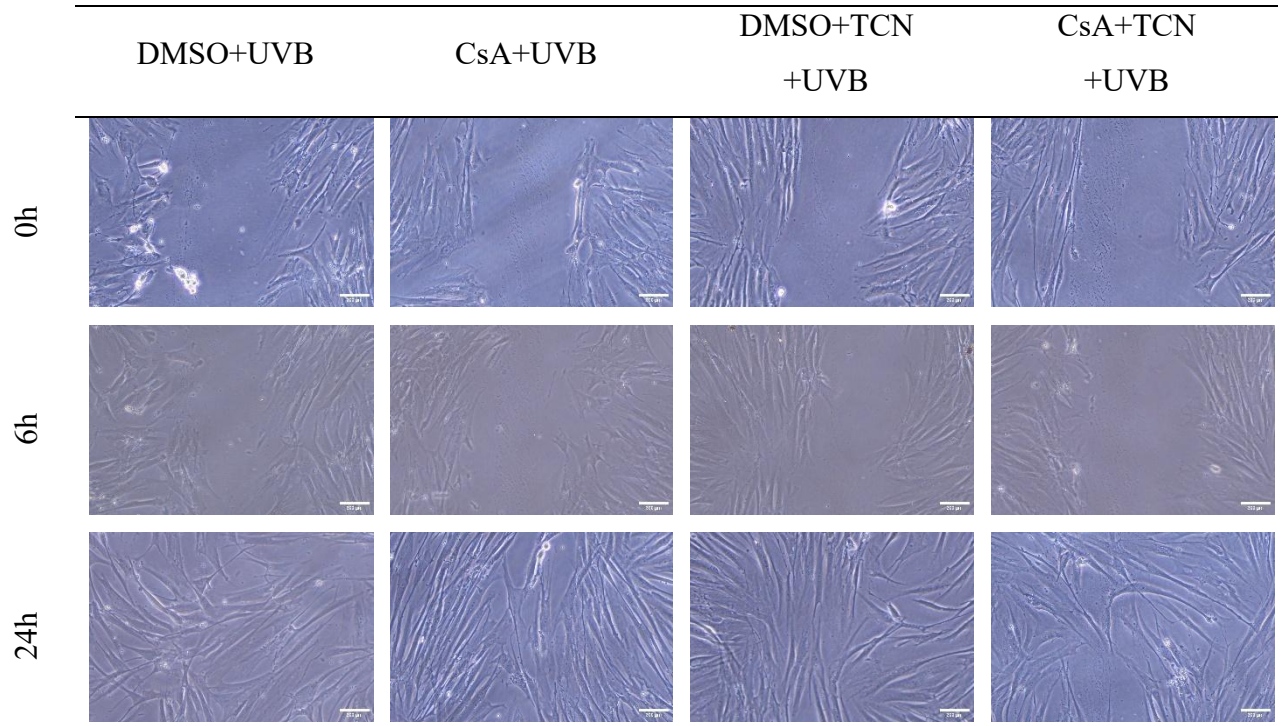

Figure 30: Time-course analysis of fibroblasts cell migratory capacity under combined UVB and pharmacological treatments. Representative images of monolayers at 0-, 6-, and 24- hours post-scratch. The images illustrate treatment-dependent differences in gap closure over time. Scale bar represents 300µm.

Following UVB irradiation, cell migration was further assessed in fibroblasts (Figure 30). Across all conditions, the cultures demonstrated remarkable resilience to UVB exposure. At after 6 and 24 hours, only minimal cell debris was visually observed, and the scratch area was nearly closed in all treatments. This contrasts sharply with HaCaT keratinocytes, where UVB exposure, especially in combination with TCN, led to significant disruption and cell detachment in the TCN+UVB (Figure 18). As observed with fibroblasts, both DMSO and CsA cultures exposed to UVB showed efficient migration and maintained monolayer integrity, indicating that short-term UVB exposure at this dose did not significantly impair cellular motility. Similarly, TCN-treated culture combined with CsA and UVB also only exhibited a slight delay in gap closure, with no major damage or detachment.

Altogether, fibroblast cultures demonstrated migratory capacity and resilience across all treatment conditions. TCN induced only mild delays in gap closure without compromising monolayer integrity, suggesting good tolerance to short-term exposure to both agents. Following UVB irradiation, the cells maintained efficient migration, contrasting with the more vulnerable response observed in keratinocytes.

4. Discussion

This study provides a comprehensive overview of keratinocyte and fibroblast responses to pharmacological and environmental stressors, focusing on short-term effects in 2D monolayer cultures. Specifically, it investigates how CsA, UVB, and the kinase inhibitor TCN influence cellular processes such as gene expression, migration, and extracellular matrix remodeling. These insights are particularly relevant given the increased risk of cSCC observed in patients receiving long-term CsA therapy combined with UV exposure. CsA's modulation of stress and signaling pathways in keratinocytes may contribute to enhanced tumorigenic potential under UVB-induced damage, emphasizing the clinical importance of dissecting these molecular mechanisms.

4.1 Gene expression changes in HaCaT

4.1.1 CsA enhances ATF3 expression under UVB or kinase inhibition

AKT1, NFATc1, and ATF3 displayed different transcriptional responses to the various treatments in HaCaT. CsA alone did not significantly alter the expression of these genes, whereas UVB exposure led to upregulation of all three. Specifically, AKT1 remained largely unchanged, showing only a slight increase following UVB exposure (Figure 7). In contrast, transcription of NFATc1 was elevated under multiple conditions, including UVB, CsA+UVB, TCN, CsA+TCN and TCN+UVB (Figure 8). ATF3, known as an immediate early gene responsive to cellular stressors such as UVB radiation, was also upregulated in this experiment (Figure 9).

NFATc1, a calcium-dependent transcription factor central to immune signaling, keratinocyte proliferation, and migration, was consistently induced under stress (Figure 8). This pattern aligns with previous reports linking NFATc1 to enhancer-driven activation during cellular injury[90,96]. Notably, NFATc1 has been shown to repress ATF3 transcription in keratinocytes[97], suggesting a regulatory interplay between these factors. This repression may be particularly relevant under TCN treatments, as reflected by comparative expression patterns in Figure 8 and Figure 9.

UVB-induced ATF3 expression has been associated with DNA damage response and apoptosis regulation, acting as a protective mechanism against stress[98,99]. In line with this, CsA-treated keratinocytes also showed elevated levels of ATF3 (Figure 9), especially when combined with

TCN inhibitor or UVB, indicating that calcineurin and kinase inhibition may collaboratively amplify ATF3-mediated stress signaling.

In summary, while CsA alone did not significantly alter the transcription of AKT1, NFATc1, or ATF3, its combination with UVB or TCN resulted in pronounced transcriptional changes. NFATc1 was consistently induced under stress, while ATF3 was upregulated when NFAT-mediated repression was relieved by CsA and TCN. As a stress-responsive factor, ATF3's increased expression under CsA+UVB and CsA+TCN suggests an amplified stress signaling response, potentially influencing keratinocyte stress adaptation and tumorigenic potential. These findings align with established mechanisms by which CsA and UVB, both independently and in combination, reinforce stress and signaling networks in keratinocytes via NFATc1-ATF3 axis[97,100].

4.1.2 Lack of EMT signature under CsA treatment in 2D culture

Of all the EMT-relevant genes analyzed, CDH1 was upregulated under all stress conditions, with the highest expression observed in CsA+TCN+UVB and UVB groups (Figure 10). CDH2 only showed increased expression following UVB exposure but was downregulated by TCN and the combined treatments (Figure 11). ZEB1 remained virtually stable or was downregulated, with the most notable downregulation seen in CsA+UVB and TCN+UVB conditions (Figure 12).

These expression profiles collectively suggest that EMT is not induced in HaCaT cells under CsA treatment in 2D culture within the experimental timeframe. Contrary to previous studies of CsA-induced EMT[38,74], CDH1 was consistently upregulated, while CDH2 and ZEB1 were unchanged. The upregulation of CDH1, especially under UVB exposure, contrasts with previous reports in which UVB exposure typically leads to CDH1 decrease associated with apoptosis and reduced adhesion[101,102]. However, in this study, the UVB dose (250 J/m^2) was relatively low[103,104], and the exposure duration to stress factor was limited to three days, with cells harvested 24 hours post-irradiation. These factors may have mitigated the typical UVB-induced stress response, allowing for a compensatory or delayed upregulation of CDH1. Previous studies suggest that exposing HaCaT cells to UVB doses between 300 and 600 J/m^2 reliably induce photodamage and photoaging, while doses near 400-500 J/m^2 are typically used to reproduce cellular stress responses[103,104]. Additionally, the 2D culture system may not fully recapitulate the dynamic cell-cell interactions and structural remodeling seen in 3D models, potentially influencing the epithelial

marker expression profile. Thus, the increased CDH1 expression in this experiment may reflect a transient epithelial reinforcement rather than a canonical EMT response.

4.1.3 Selective activation of TGF-β pathway preserves epithelial stability

In barrier tissues like the skin, TGFB1 plays a critical role in regulating inflammation and maintaining epithelial integrity following environmental insults like UVB irradiation. The analysis of SMAD2, SMAD3, SMAD4, and TGFB1 revealed differential transcriptional responses to UVB and TCN treatments (e.g. for SMAD2), reflecting selective activation within the canonical signaling pathway (Figure 14).

This selective activation likely reflects TGFB1's dual role as both a stress-responsive cytokine and a tumor suppressor. In early-stage tumor or non-transformed cells, TGFB1 promotes cell cycle arrest, apoptosis, and tissue repair[69,70,79,105], thereby suppressing tumor initiation. However, in advanced malignancies, it may shift toward a tumor-promoting role[69,106]. The short-term, low-dose exposure used in this study may have favored TGFB1's homeostatic and reparative functions rather than its pro-EMT role observed in chronic or tumorigenic contexts. The absence of coordinated SMAD2/3/4 activation further supports the idea that TGF-β signaling was not fully engaged, potentially contributing to epithelial repair without driving EMT. This selective activation may reflect the balance between maintaining epithelial integrity and initiating stress adaptation under combined treatment conditions.

4.1.4 ECM-related transcriptional changes highlight stress adaptation in keratinocytes

The ECM related genes COL7A1, MMP2, and MMP9 showed varied transcriptional responses to stress treatment. COL7A1 was consistently upregulated across all conditions, with moderate change under CsA alone and markedly higher expression in CsA+TCN+UVB (Figure 15). MMP2 was slightly increased, with further increases observed in combined CsA treatments involving TCN and TCN+UVB. MMP9 displayed a pronounced, condition-dependent increase, peaking under TCN+UVB treatment (Figure 16).

These expression patterns indicate a strong transcriptional response related to ECM remodeling and tissue repair in HaCaT cells exposed to UVB and TCN. MMP9 is known to be induced by UVB and oxidative stress, and its overexpression in skin is associated with inflammatory responses and epithelial damage[107–109]. Interestingly, CsA-treated cultures showed elevated but

comparatively lower MMP9 expression, suggesting that CsA may regulate inflammatory signaling and preserve cell adhesion. The coordinated upregulation of COL7A1 alongside MMPs highlights the dual nature of the cellular response, both disruptive and reparative, depending on the treatment context. These data suggest that while UVB and TCN promote ECM degradation and remodeling, CsA may buffer this effect, supporting epithelial adherence and structural integrity under stress.

Overall, the findings of gene expression changes in HaCaT cell line depict CsA as a modulator that supports keratinocyte stress adaptation by enhancing specific stress signaling axis (NFATc1-ATF3), mitigating excessive EMT and ECM degradation, and preserving epithelial and matrix integrity under UVB and TCN.

4.2 Interplay between CsA, UVB and kinase inhibition in regulating cell movement

This study investigated the effects of CsA on keratinocytes migration under UVB-induced stress. Contrary to previous reports suggesting CsA promotes migration via Akt/mTOR activation[38], our findings indicate that CsA reduced HaCaT cell migration and increased cellular damage when combined with UVB in short-term 2D assay. This discrepancy may be attributed to stress-inducing effects overriding pro-migratory signaling, particularly in the simplified 2D culture system. The absence of stromal interactions and basement membrane components may further limit the manifestation of CsA's full effect on cell movement. Additionally, the result may reflect previous findings indicate that CsA alone does not robustly induce Akt phosphorylation[38], a key regulator of migration and invasion. Longer treatment durations or a 3D environment may be necessary to fully capture CsA's impact on cell movement.

The presence of cellular debris (Supplementary Figure S3) reflects increased cell stress or early cytotoxicity under combined CsA and UVB treatment, potentially counteracting any migratory acceleration expected from CsA's modulation of Akt/mTOR under normal conditions. Despite low transcriptional levels of Akt, its functional activation might still be significant. This possibility warrants further investigation, particularly through assays targeting phosphorylated Akt, to clarify the relationship between CsA treatment and Akt-mediated migratory signaling.

In keratinocytes, UVB irradiation significantly delayed migration, reduced gap closure in vitro and impaired adhesion crucial for cell movement (Figure 18). While CsA alone did not enhance

migration as anticipated, its combination with TCN significantly suppressed motility (Figure 17). This suggests that CsA's pro-migratory effect likely depends on functional Akt signaling, which is inhibited by TCN. However, cells exposed to TCN alone retained some migratory capacity, possibly via alternative pathways like MAPK (Figure 2). Under CsA+TCN, these alternative pathways may not sufficiently compensate, explaining the suppressed migration.

These findings illuminate the complex interplay of pharmacological and environmental stressors on keratinocyte behavior, emphasizing the need for further studies to dissect underlying signaling networks.

4.3 Gene expression changes in fibroblast

4.3.1 Selective transcriptional responses in fibroblasts highlight context-dependent stress sensitivity

The expression of stress-responsive genes (AKT1, NFATc1, and ATF3) indicates that fibroblasts exhibit a more subdued and selective stress gene activation profile compared to keratinocytes. These findings also highlight the importance of cell-type-specific sensitivity and spatial context in interpreting UVB-induced signaling dynamics.

The paradoxical increase observed in AKT1 expression under TCN treatment may reflect a compensatory transcriptional response, in which the inhibition of Akt phosphorylation by TCN could trigger feedback mechanisms that upregulate AKT1 expression in an attempt to restore signaling balance[110]. In CsA-treated fibroblasts, AKT1 levels were consistently lower than baseline. These results suggest that while TCN may enhance AKT1 expression in isolation, both UVB and CsA at the tested doses appear to attenuate its transcription (Figure 19).

The observed downregulation of NFATc1 in fibroblast, particularly under CsA+UVB treatment (Figure 20), suggests a compounded suppression of transcription through both pharmacological and environmental stimuli. While CsA is known to inhibit calcineurin-dependent NFAT activation, the additional repression of UVB may reflect broader stress-induced signaling disruptions.

The expression of ATF3 in CsA was only slightly elevated (Figure 21), suggesting that fibroblasts may possess distinct regulatory threshold for ATF3 activation, requiring more sustained or intense stress stimuli to elicit a robust transcriptional response[111,112].

In summary, fibroblasts display a more restrained and selective activation of stress-responsive genes (AKT1, NFATc1, ATF3) compared to keratinocytes, highlighting cell-type-specific sensitivities and spatial context effects in UVB-induced signaling.

4.3.2 Stable mesenchymal profile with activated features in stressed fibroblasts

The analysis of the EMT genes expression suggests that fibroblasts, while inherently mesenchymal, undergo further modulation of EMT-related markers under combined stress conditions rather than EMT transition. The observed changes likely reflect a shift toward a more activated fibroblast phenotype (Figure 25), relevant in contexts such as wound healing, fibrosis, and stromal remodeling in UVB-exposed, drug-modulated skin. The largely unchanged ZEB1 expression further supports the idea that EMT regulation in fibroblasts under these conditions is driven more by cadherin dynamics than transcriptional reprogramming[113]. Rather than undergoing a phenotypic switch, fibroblasts appear to reinforce or fine-tune their mesenchymal characteristics in response to the tested stress factors.

4.3.3 CsA and kinase inhibition cooperatively engage TGF-β signaling in fibroblasts

Gene expression analysis of the TGF-β signaling pathway revealed that TCN, especially in combination with CsA, triggered coordinated upregulation of SMAD2, SMAD3 and SMAD4 (Figure 26). This pattern is consistent with activation of the canonical TGF-β pathway and suggests a transcriptional response associated with fibroblast activation. The strong induction of SMAD3 and TGFB1 in CsA+TCN and TCN culture, respectively, supports a role in ECM remodeling and wound repair kinetics. The co-expression of multiple SMADs alongside TGFB1 strengthens the interpretation of pathway engagement under kinase inhibition.

In contrast, isolated or minimal changes in SMADs under UVB suggest that UVB exposure does not robustly activate the TGF-β pathway in fibroblasts under the conditions tested. These findings align with the known role of TGF-β signaling in fibroblast differentiation, migration, and ECM production[114], and may reflect a stress-adaptive response to kinase inhibition (e.g. via TCN) and pharmacological stress (e.g. CsA) signaling[115].

4.3.4 Fibroblast ECM gene expression indicates stress-driven remodeling dynamics

Gene expression analysis of ECM remodeling markers suggests that TCN elicits a dual ECM remodeling response in fibroblasts, enhancing matrix production via COL7A1 (Figure 27) while

simultaneously promoting matrix turnover through MMP9 (Figure 28). This is consistent with the activation of TGF-β signaling observed in earlier results (Figure 26) and may reflect a stress-adaptive or reparative phenotype. Interestingly, the selective downregulation of MMP2, particularly under UVB and combined treatments, may indicate a shift toward matrix preservation, potentially serving to prevent excessive degradation. Notably, MMP9 is known to be highly responsive to stress signals, facilitating cell migration by degrading type IV collagen[116–118]. In contrast, MMP2 also targets other collagen subtypes and is more associated with structural remodeling[117]. Its suppression may serve to prevent excessive matrix breakdown under acute stress. Although MMP2 was not directly assessed in 3D OTC system, MMP9 expression in fibroblast OTC was reduced upon CsA treatment[38]. Our findings differ from those observed in 3D OTCs and highlight the context-dependent regulation of ECM remodeling genes, underscoring the importance of model systems in interpreting fibroblast behavior.

4.4 CsA and UVB preserve fibroblast motility, while TCN slightly inhibit cell movement

Migration assay results demonstrate that fibroblasts retain strong migratory capacity under short-term CsA and TCN exposure, with only minor delays observed in TCN-treated conditions (Figure 29). Even under combined stress from CsA, UVB, and TCN, the cells maintained their function and monolayer integrity, with minimal cytotoxic effects (Figure 30). This resilience contrasts with the more pronounced stress responses observed in HaCaT cells, highlighting cell-type-specific differences in migration and stress adaptation.

These findings suggest that fibroblasts may play a stabilizing role in skin remodeling under pharmacological and environmental stress, contributing to wound healing and matrix maintenance. Their ability to preserve cell motility and structural integrity under combined treatments underscore their importance in maintaining tissue homeostasis during injury or therapeutic intervention.

4.5 2D culture responses: stress adaptation without signs of invasion

The 2D HaCaT culture system effectively captured early transcriptional and phenotypic responses to stress, including changes in gene expression and cell motility. While treatments such as CsA, UVB, and TCN induced signs of cellular stress and modulated adhesion, the observations indicate

that the cell remained in a migratory state and far from acquiring enhanced motility characteristics. The inhibition of migration under combined stress conditions may have prevented progression toward EMT-like behavior, further supporting the conclusion that the observed responses reflect early-stage, adaptive mechanisms rather than malignant transformation.

Additionally, migration assays further revealed monolayer disruption and widespread cell detachment in TCN+UVB culture. This morphological outcome is consistent with the expression of ECM remodeling genes observed after TCN+UVB treatment, in which MMP9 expression is higher (Figure 16). CsA appeared to buffer this effect, supporting cell adhesion and structural stability. The outcomes reinforce the idea that CsA appears to enhance cell-substrate interaction, possibly by modulating ECM composition or adjusting stress signaling pathways, thereby supporting survival under acute UVB exposure, potentially more evident at later timepoints.

In contrast, fibroblasts exhibited robust motility and maintained monolayer integrity across all treatment conditions. While TCN caused a slight delay in migration, no significant cytotoxicity or detachment was observed. This mild impairment aligns with the transcriptional activation of ECM remodeling and stress-responsive pathways under TCN treatment. Gene expression analysis revealed selective engagement of the TGF-β/SMAD pathway, particularly under TCN treatment, with upregulation of TGFB1, SMAD3, and COL7A1, alongside MMP9. These changes suggest a stress-adaptive or reparative phenotype, consistent with early ECM remodeling and fibroblast activation. The consistency between functional and molecular findings highlights TCN as a potential key regulator of fibroblast behavior.

4.6 Comparison with 3D organotypic cultures

While 2D cultures captured early transcriptional and migratory responses, 3D OTCs could reveal more complex structural remodeling and invasive phenotypes. In HaCaT OTCs, CsA activated the Akt/mTOR pathway, leading to invasion into the dermis and degradation of basement membrane components such as Collagen VII[38]. This degradation appeared to be post-transcriptional, as it was not reflected in gene expression levels, suggesting destabilization at the protein level.

TCN as Akt inhibitor, successfully blocked CsA-induced invasion, confirming the role of Akt signaling in mediating this behavior. However, following exposure to solar-simulated irradiation,

TCN failed to prevent invasion, indicating the involvement of additional pathways, such as TGF-β, in driving invasive responses[38].

Fibroblasts within OTCs exhibited morphological changes and matrix reorganization, contributing to a tumor-permissive microenvironment. Gene expression profiles suggested myofibroblast-like differentiation, although this was not confirmed at the protein level. Our findings from 2D cultures indicated that cells remained adherent with no evident morphological alterations, despite showing transcriptional signs of activation. This discrepancy underscores the limitation of 2D system in capturing the dynamic phenotypic plasticity and cell-matrix interactions essential for fibroblast activation. Differences between 2D and 3D systems were also evident in ECM component regulation. While COL7A1 was upregulated in 2D culture under stress, it was degraded in 3D OTCs, particularly at invasion sites.

Together, these findings underscore the value of complementary 3D models in capturing invasive and remodeling behaviors relevant to cancer progression under pharmacological and environmental stress. The integration of both systems, as summarized in Supplementary Table S1, provides a more comprehensive understanding of keratinocyte and fibroblast responses, bridging molecular signaling to functional cellular adaptations and stress-induced remodeling.

4.7 Conclusions and future directions

The findings from 2D cultures suggest that short-term exposure to CsA, TCN, and UVB induces adaptive stress responses in both keratinocytes and fibroblasts, without triggering full EMT or invasive transformation. However, the absence of stratification, dermal-epidermal junctions, and tissue architecture limits the interpretation of these results as true normalization or transformation. Unlike in OTCs, where CsA induced visible tissue rearrangements interpreted as epidermal normalization, the 2D system primarily reflects maintenance of epithelial features under stress.

This study demonstrates that 2D cultures are effective for capturing early transcriptional and migratory responses, while 3D models are essential for revealing structural remodeling and invasive behavior. The complementary insights from both systems could enhance our understanding of how CsA, TCN, and UVB modulate skin cell behavior, with broader implications for wound healing mechanisms, fibrosis, and carcinogenesis in immunosuppressed environments.

Comparative analysis with the literature on 3D organotypic cultures further highlights the limitations of 2D systems in fully recapitulating invasive transformation and ECM degradation. Nonetheless, 2D assays effectively reflect early-stage adaptation and cell-matrix interactions. The findings provide new insights into the interplay between CsA, UVB, and cell-specific signaling pathways, underscoring the complexity of skin carcinogenesis in immunosuppressed patients. Overall, this work advances the mechanistic understanding of skin cell responses to pharmacological and environmental stress, laying the foundation for future studies on chronic adaptation, invasive transformation, and dermal-epidermal dynamics in cancer and wound healing contexts.

To build on these findings, future studies could extend exposure durations to evaluate delayed EMT or invasive behavior. Additionally, miRNA profiling may uncover post-transcriptional regulatory networks involved in stress adaptation and transformation. Protein-level validation using techniques such as ELISA or western blotting would help confirm myofibroblast differentiation and support transcriptional data.

While UVB was used in this study to model environmental stress relevant to skin carcinogenesis, it is important to note that UVB has limited dermal penetration. To better assess fibroblast-specific responses and their role in shaping the tumor microenvironment, future investigations may consider incorporating UVA exposure. UVA penetrates deeper into the skin and may more accurately simulate chronic photodamage experienced in vivo. This approach could provide a more comprehensive understanding of fibroblast contributions to carcinogenesis in immunosuppressed skin, particularly in the context of long-term CsA treatment and chronic UV exposure.

Supplementary

Supplementary Table S1 Summary of gene expression and phenotypic responses across 2D HaCaT, 2D fibroblasts, and 3D OTCs.

Marker/Pathway	2D HaCaT	2D Fibroblast	3D OTCs[38]
AKT1	Stable, post-transcriptional regulation	Upregulated by TCN, inactive under UVB/CsA	Activated by CsA, promotes invasion, blocked by TCN
NFATc1	Induced by UVB/TCN, Suppressed by CsA	Downregulated	Not assessed
ATF3	Elevated under UVB/TCN, Activated by CsA	Mildly activated by CsA	Not assessed
EMT markers	Epithelial maintenance	Activated mesenchymal phenotype	Collective invasion
TGFB/SMAD pathway	TGFB1, SMAD3/4 elevated as reparative mechanism	Fibroblasts activation via canonical pathway	Activated supporting fibroblast remodeling
COL7A1 (Collagen VII)	Matrix reinforcement	Strongly induced by TCN	Degraded by CsA, Redistributed in matrix
MMP2	Moderately induced	Generally suppressed	Not assessed, Matrix degradation observed
MMP9	Strongly expressed under TCN+UVB, buffered by CsA	Matrix turnover, activated across all conditions	Downregulated in fibroblasts, No protein change
Migration behavior	Reduced by CsA/TCN/UVB or combination	Robust migratory activity	HaCat invasion promoted by CsA and fibroblast rounding near invasion site

Supplementary Table S2 Summary of unpaired t-test and adjusted p-values for HaCaT and fibroblast across treatments. Values with p < 0.05 are highlighted in bold, with asterisk (*) indicating significance. Only TGFB1 under TCN treatment in fibroblasts remained significant post-correction. This table complements the qPCR methodology in the method section.

HaCaT					Fibroblast				
Treatment	**Gene**	**t.test**	**p.value**	**adj.p.value**	**Treatment**	**Gene**	**t.test**	**p.value**	**adj.p.value**
CSA	AKT1	0.388	0.701	>0.999	CSA	AKT1	0.573	0.571	>0.999
CSA	ATF3	-0.193	0.849	>0.999	CSA	ATF3	-0.825	0.417	>0.999
CSA	CDH1	-0.843	0.407	>0.999	CSA	CDH1	-0.111	0.913	>0.999
CSA	CDH2	0.197	0.845	>0.999	CSA	CDH2	-0.828	0.415	>0.999
CSA	COL7A1	-1.373	0.182	>0.999	CSA	COL7A1	0.569	0.574	>0.999
CSA	MMP2	-0.220	0.828	>0.999	CSA	MMP2	0.912	0.370	>0.999
CSA	MMP9	-1.310	0.203	>0.999	CSA	MMP9	-1.060	0.298	>0.999
CSA	NFATc1	-0.247	0.807	>0.999	CSA	NFATc1	0.787	0.438	>0.999
CSA	SMAD2	0.282	0.780	>0.999	CSA	SMAD2	-1.560	0.130	>0.999
CSA	SMAD3	-0.112	0.912	>0.999	CSA	SMAD3	-0.452	0.655	>0.999
CSA	SMAD4	0.014	0.989	>0.999	CSA	SMAD4	-0.763	0.452	>0.999
CSA	TGFB1	-0.748	0.462	>0.999	CSA	TGFB1	0.739	0.466	>0.999
CSA	ZEB1	0.194	0.848	>0.999	CSA	ZEB1	-0.162	0.873	>0.999
CSA+TCN	AKT1	0.632	0.534	>0.999	CSA+TCN	AKT1	0.294	0.771	>0.999
CSA+TCN	ATF3	-1.370	0.183	>0.999	CSA+TCN	ATF3	-0.010	0.992	>0.999
CSA+TCN	CDH1	-1.757	0.091	>0.999	CSA+TCN	CDH1	0.135	0.894	>0.999
CSA+TCN	CDH2	0.747	0.462	>0.999	**CSA+TCN**	**CDH2**	**-2.267**	**0.031**	**0.502**
CSA+TCN	**COL7A1**	**-3.184**	**0.004**	**0.062**	**CSA+TCN**	**COL7A1**	**-2.078**	**0.047**	**0.752**
CSA+TCN	MMP2	-1.713	0.099	>0.999	CSA+TCN	MMP2	-0.490	0.629	>0.999
CSA+TCN	**MMP9**	**-2.836**	**0.009**	**0.151**	CSA+TCN	MMP9	-1.933	0.064	>0.999
CSA+TCN	NFATc1	-1.508	0.144	>0.999	CSA+TCN	NFATc1	0.841	0.407	>0.999
CSA+TCN	SMAD2	0.541	0.593	>0.999	**CSA+TCN**	**SMAD2**	**-2.221**	**0.035**	**0.554**
CSA+TCN	SMAD3	-1.707	0.100	>0.999	**CSA+TCN**	**SMAD3**	**-2.746**	**0.011**	**0.174**
CSA+TCN	SMAD4	-1.648	0.112	>0.999	CSA+TCN	SMAD4	-1.626	0.115	>0.999
CSA+TCN	TGFB1	-1.854	0.076	>0.999	CSA+TCN	TGFB1	-1.231	0.229	>0.999
CSA+TCN	ZEB1	0.436	0.667	>0.999	CSA+TCN	ZEB1	-0.931	0.360	>0.999
CSA+UVB	AKT1	0.245	0.808	>0.999	CSA+UVB	AKT1	1.250	0.222	>0.999
CSA+UVB	ATF3	-1.187	0.247	>0.999	CSA+UVB	ATF3	-0.230	0.820	>0.999
CSA+UVB	CDH1	-1.895	0.070	>0.999	CSA+UVB	CDH1	1.241	0.226	>0.999

CSA+UVB	CDH2	-0.262	0.796	>0.999	CSA+UVB	CDH2	0.442	0.662	>0.999
CSA+UVB	**COL7A1**	**-2.846**	**0.009**	**0.140**	CSA+UVB	COL7A1	-0.790	0.436	>0.999
CSA+UVB	MMP2	-1.031	0.313	>0.999	CSA+UVB	MMP2	1.554	0.132	>0.999
CSA+UVB	MMP9	-1.951	0.064	>0.999	CSA+UVB	MMP9	-0.807	0.427	>0.999
CSA+UVB	NFATc1	-1.463	0.156	>0.999	**CSA+UVB**	**NFATc1**	**2.404**	**0.023**	**0.370**
CSA+UVB	SMAD2	-0.179	0.860	>0.999	CSA+UVB	SMAD2	-0.622	0.539	>0.999
CSA+UVB	SMAD3	-0.043	0.966	>0.999	CSA+UVB	SMAD3	-0.046	0.963	>0.999
CSA+UVB	SMAD4	-0.930	0.361	>0.999	CSA+UVB	SMAD4	-0.310	0.759	>0.999
CSA+UVB	TGFB1	-1.156	0.259	>0.999	CSA+UVB	TGFB1	0.608	0.548	>0.999
CSA+UVB	**ZEB1**	**2.822**	**0.009**	**0.148**	CSA+UVB	ZEB1	-0.191	0.850	>0.999
CSA+TCN+UVB	AKT1	0.585	0.564	>0.999	CSA+TCN+UVB	AKT1	0.353	0.727	>0.999
CSA+TCN+UVB	ATF3	-1.209	0.238	>0.999	CSA+TCN+UVB	ATF3	-0.046	0.964	>0.999
CSA+TCN+UVB	**CDH1**	**-2.328**	**0.028**	**0.454**	**CSA+TCN+UVB**	**CDH1**	**2.509**	**0.019**	**0.296**
CSA+TCN+UVB	CDH2	1.780	0.087	>0.999	CSA+TCN+UVB	CDH2	-0.416	0.681	>0.999
CSA+TCN+UVB	**COL7A1**	**-3.253**	**0.003**	**0.053**	CSA+TCN+UVB	COL7A1	-1.631	0.114	>0.999
CSA+TCN+UVB	MMP2	-1.852	0.076	>0.999	CSA+TCN+UVB	MMP2	0.963	0.345	>0.999
CSA+TCN+UVB	**MMP9**	**-3.155**	**0.005**	**0.072**	CSA+TCN+UVB	MMP9	-1.166	0.254	>0.999
CSA+TCN+UVB	NFATc1	-0.396	0.696	>0.999	CSA+TCN+UVB	NFATc1	0.267	0.792	>0.999
CSA+TCN+UVB	SMAD2	0.410	0.686	>0.999	CSA+TCN+UVB	SMAD2	-1.106	0.278	>0.999
CSA+TCN+UVB	SMAD3	-1.563	0.131	>0.999	CSA+TCN+UVB	SMAD3	-1.463	0.156	>0.999
CSA+TCN+UVB	SMAD4	-1.293	0.208	>0.999	CSA+TCN+UVB	SMAD4	-0.330	0.744	>0.999
CSA+TCN+UVB	TGFB1	-1.615	0.119	>0.999	CSA+TCN+UVB	TGFB1	-1.783	0.086	>0.999
CSA+TCN+UVB	ZEB1	1.723	0.097	>0.999	CSA+TCN+UVB	ZEB1	-0.006	0.995	>0.999
TCN	AKT1	-0.608	0.549	>0.999	TCN	AKT1	-0.707	0.486	>0.999
TCN	ATF3	-0.099	0.922	>0.999	TCN	ATF3	0.711	0.483	>0.999
TCN	CDH1	-1.787	0.086	>0.999	TCN	CDH1	-0.832	0.413	>0.999
TCN	CDH2	0.257	0.799	>0.999	TCN	CDH2	-0.943	0.354	>0.999
TCN	**COL7A1**	**-2.362**	**0.026**	**0.422**	**TCN**	**COL7A1**	**-2.967**	**0.006**	**0.098**
TCN	MMP2	-1.186	0.247	>0.999	TCN	MMP2	0.241	0.811	>0.999
TCN	**MMP9**	**-3.132**	**0.005**	**0.076**	**TCN**	**MMP9**	**-2.378**	**0.025**	**0.392**
TCN	NFATc1	-1.050	0.304	>0.999	TCN	NFATc1	0.272	0.788	>0.999
TCN	SMAD2	2.056	0.051	0.809	TCN	SMAD2	-1.663	0.108	>0.999
TCN	SMAD3	-1.131	0.269	>0.999	TCN	SMAD3	-1.117	0.274	>0.999

TCN	SMAD4	-1.137	0.266	>0.999	TCN	SMAD4	-0.741	0.465	>0.999
TCN	TGFB1	-1.728	0.097	>0.999	**TCN**	**TGFB1**	**-3.524**	**0.002**	**0.0239 (*)**
TCN	ZEB1	-0.105	0.917	>0.999	TCN	ZEB1	-0.086	0.932	>0.999
UVB	AKT1	-1.349	0.190	>0.999	UVB	AKT1	0.499	0.622	>0.999
UVB	ATF3	-1.613	0.120	>0.999	UVB	ATF3	0.450	0.657	>0.999
UVB	**CDH1**	**-2.413**	**0.024**	**0.378**	UVB	CDH1	-0.420	0.678	>0.999
UVB	CDH2	-1.445	0.161	>0.999	UVB	CDH2	-0.135	0.894	>0.999
UVB	**COL7A1**	**-2.429**	**0.023**	**0.364**	UVB	COL7A1	-1.809	0.081	>0.999
UVB	MMP2	-1.039	0.309	>0.999	UVB	MMP2	-0.447	0.659	>0.999
UVB	MMP9	-1.893	0.071	>0.999	UVB	MMP9	-0.038	0.970	>0.999
UVB	NFATc1	-1.474	0.153	>0.999	UVB	NFATc1	-0.007	0.994	>0.999
UVB	SMAD2	-0.098	0.923	>0.999	UVB	SMAD2	-1.128	0.269	>0.999
UVB	SMAD3	-0.878	0.388	>0.999	UVB	SMAD3	-1.464	0.155	>0.999
UVB	SMAD4	-1.137	0.266	>0.999	UVB	SMAD4	-0.555	0.584	>0.999
UVB	TGFB1	-1.815	0.082	>0.999	UVB	TGFB1	-1.430	0.164	>0.999
UVB	ZEB1	0.089	0.930	>0.999	UVB	ZEB1	-0.353	0.727	>0.999
TCN+UVB	AKT1	-0.370	0.715	>0.999	TCN+UVB	AKT1	1.782	0.086	>0.999
TCN+UVB	ATF3	0.197	0.845	>0.999	TCN+UVB	ATF3	0.644	0.525	>0.999
TCN+UVB	**CDH1**	**-2.089**	**0.047**	**0.754**	TCN+UVB	CDH1	0.776	0.444	>0.999
TCN+UVB	CDH2	0.708	0.485	>0.999	TCN+UVB	CDH2	0.911	0.370	>0.999
TCN+UVB	**COL7A1**	**-2.855**	**0.009**	**0.137**	TCN+UVB	COL7A1	0.721	0.477	>0.999
TCN+UVB	MMP2	-1.137	0.266	>0.999	TCN+UVB	MMP2	1.919	0.066	>0.999
TCN+UVB	**MMP9**	**-2.897**	**0.008**	**0.131**	TCN+UVB	MMP9	0.822	0.418	>0.999
TCN+UVB	NFATc1	-1.708	0.100	>0.999	TCN+UVB	NFATc1	1.115	0.274	>0.999
TCN+UVB	SMAD2	1.317	0.200	>0.999	TCN+UVB	SMAD2	0.334	0.741	>0.999
TCN+UVB	SMAD3	-1.603	0.122	>0.999	TCN+UVB	SMAD3	-0.658	0.517	>0.999
TCN+UVB	SMAD4	-1.766	0.090	>0.999	TCN+UVB	SMAD4	0.067	0.947	>0.999
TCN+UVB	TGFB1	-2.056	0.051	0.808	TCN+UVB	TGFB1	0.259	0.798	>0.999
TCN+UVB	**ZEB1**	**3.103**	**0.005**	**0.076**	TCN+UVB	ZEB1	1.114	0.275	>0.999

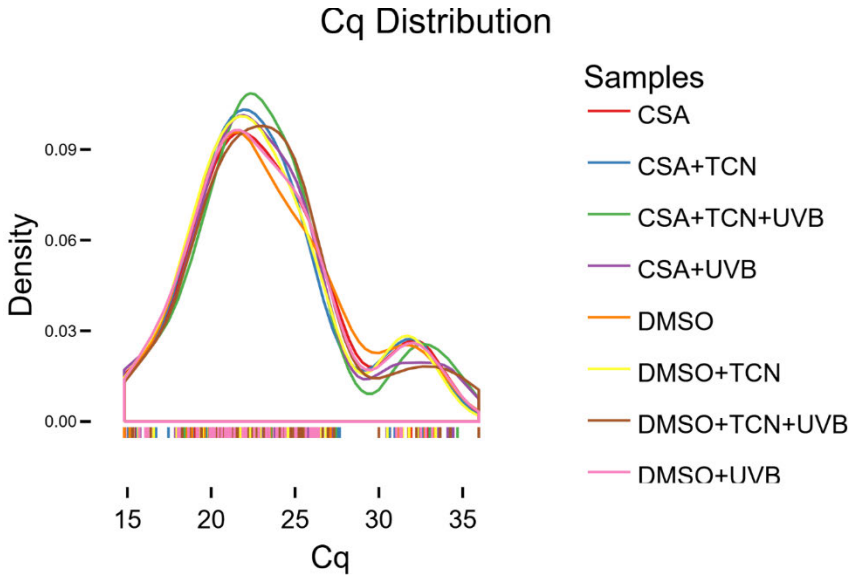

Supplementary Figure S1: Distribution of Ct values in HaCaT across eight treatments. The density plot illustrates the variation in quantification cycle values for each condition. This visualization provides an overview of amplification consistency and Ct range across eight experimental groups. The presence of a secondary peak likely reflects late-amplifying target gene ZEB1, which consistently showed low expression levels.

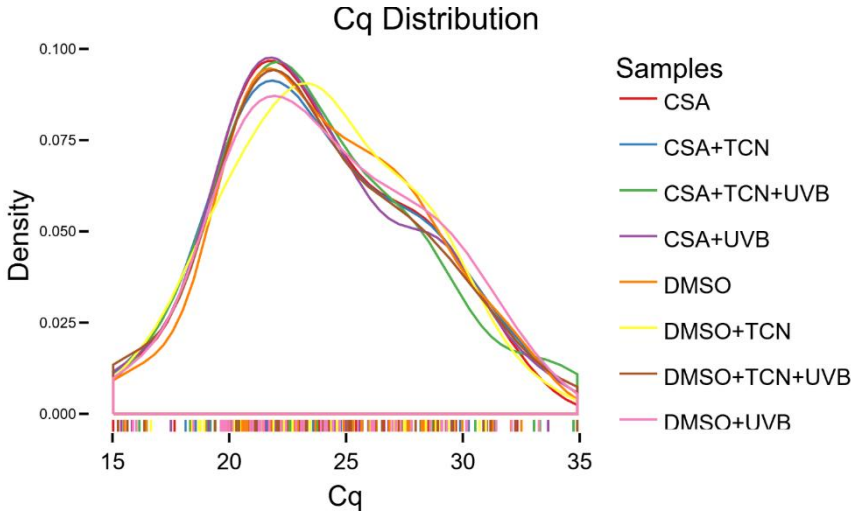

Supplementary Figure S2: Distribution of Ct values in fibroblast across eight treatments. The density plot illustrates the variation in quantification cycle values for each condition. Most distribution peak between Ct 20-25, indicating early amplification of highly expressed genes. Colored ticks below the curves represent individual data points. The absence of a distinct secondary peak suggests fewer late-amplifying gene compared to HaCaT cultures.

CsA+UVB	CsA + TCN + UVB
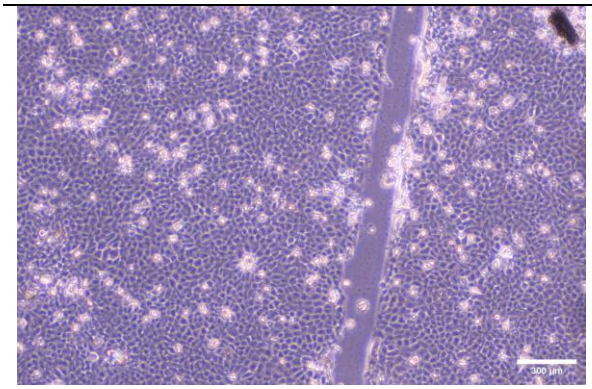	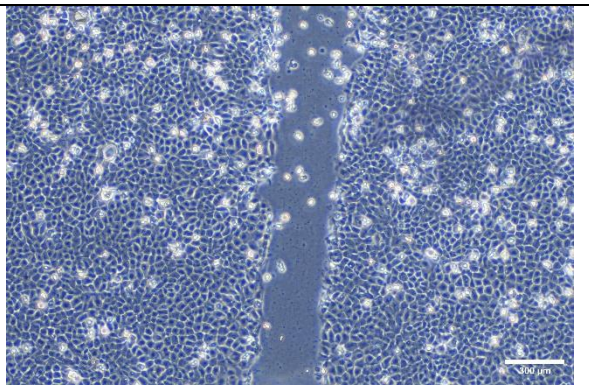

Supplementary Figure S3: Representative phase-contrast image of HaCaT cultures treated with CsA+UVB (left) and CsA+TCN+UVB (right), acquired 6-hours post UVB exposure in DMEM (left) and PBS (right). The central scratch area is visible under both conditions. Notably, scattered white particles observed in the medium are interpreted as floating cell debris, indicative of early stress responses following UVB irradiation. While debris was not the primary focus of imaging, its presence, even after replacing the culture medium, supports qualitative observations of cytotoxic effects associated with UVB and combined treatment. Scale bar represents 300µm.

References

1. Mohamed, S. A. & Hargest, R. Surgical anatomy of the skin. *Surgery (Oxford)* **40**, 1–7 (2022).
2. Abdo, J. M., Sopko, N. A. & Milner, S. M. The applied anatomy of human skin: A model for regeneration. *Wound Medicine* **28**, 100179 (2020).
3. Breitkreutz, D., Mirancea, N. & Nischt, R. Basement membranes in skin: unique matrix structures with diverse functions? *Histochem Cell Biol* **132**, 1–10 (2009).
4. Monteiro-Riviere, N. Structure and Function of Skin. in *Dermal Absorption Models in Toxicology and Pharmacology* (ed. Riviere, J.) 1–19 (CRC Press, 2005). doi:10.1201/9780203020821.ch1.
5. Hofmann, E., Schwarz, A., Fink, J., Kamolz, L.-P. & Kotzbeck, P. Modelling the Complexity of Human Skin In Vitro. *Biomedicines* **11**, 794 (2023).
6. Gallegos-Alcalá, P., Jiménez, M., Cervantes-García, D. & Salinas, E. The Keratinocyte as a Crucial Cell in the Predisposition, Onset, Progression, Therapy and Study of the Atopic Dermatitis. *IJMS* **22**, 10661 (2021).
7. Boraldi, F. *et al.* The Role of Fibroblasts in Skin Homeostasis and Repair. *Biomedicines* **12**, 1586 (2024).
8. Russo, B., Brembilla, N. C. & Chizzolini, C. Interplay Between Keratinocytes and Fibroblasts: A Systematic Review Providing a New Angle for Understanding Skin Fibrotic Disorders. *Front. Immunol.* **11**, 648 (2020).
9. Wojtowicz, A. M. *et al.* The importance of both fibroblasts and keratinocytes in a bilayered living cellular construct used in wound healing. *Wound Repair Regen* **22**, 246–255 (2014).
10. *World Cancer Report: Cancer Research for Cancer Prevention*. (International Agency for Research on Cancer, Lyon, 2020).

11. Arnold, M. *et al.* Global Burden of Cutaneous Melanoma in 2020 and Projections to 2040. *JAMA Dermatol* **158**, 495 (2022).
12. Leiter, U., Keim, U. & Garbe, C. Epidemiology of Skin Cancer: Update 2019. in *Sunlight, Vitamin D and Skin Cancer* (ed. Reichrath, J.) vol. 1268 123–139 (Springer International Publishing, Cham, 2020).
13. Giroulet, F., Tabotta, F., Pomoni, A. & Prior, J. Primary parotid Merkel cell carcinoma: a first imagery and treatment response assessment by 18F-FDG PET. *BMJ Case Rep* **12**, e226511 (2019).
14. D'Orazio, J., Jarrett, S., Amaro-Ortiz, A. & Scott, T. UV Radiation and the Skin. *IJMS* **14**, 12222–12248 (2013).
15. Schutz des Menschen vor den Gefahren solarer UV-Strahlung und UV-Strahlung in Solarien. *Die Strahlenschutzkommission* https://www.ssk.de/SharedDocs/Beratungsergebnisse/DE/2016/2016-02-11_Empf_UV-Schutz_KT.html (2016).
16. Courdavault, S. *et al.* Repair of the three main types of bipyrimidine DNA photoproducts in human keratinocytes exposed to UVB and UVA radiations. *DNA Repair* **4**, 836–844 (2005).
17. Modenese, A., Korpinen, L. & Gobba, F. Solar Radiation Exposure and Outdoor Work: An Underestimated Occupational Risk. *IJERPH* **15**, 2063 (2018).
18. El Ghissassi, F. *et al.* A review of human carcinogens—Part D: radiation. *The Lancet Oncology* **10**, 751–752 (2009).
19. Neale, R. E. *et al.* The effects of exposure to solar radiation on human health. *Photochem Photobiol Sci* **22**, 1011–1047 (2023).
20. Weller, R. B. *et al.* The effect of daily UVA phototherapy for 2 weeks on clinic and 24-h blood pressure in individuals with mild hypertension. *J Hum Hypertens* **37**, 548–553 (2022).

21. Barros, N. D. M. *et al.* Phototherapy. *Anais Brasileiros de Dermatologia* **96**, 397–407 (2021).
22. Vangipuram, R. & Feldman, S. Ultraviolet phototherapy for cutaneous diseases: a concise review. *Oral Diseases* **22**, 253–259 (2016).
23. Matsumura, Y. & Ananthaswamy, H. N. Toxic effects of ultraviolet radiation on the skin. *Toxicology and Applied Pharmacology* **195**, 298–308 (2004).
24. Smith, K. J., Hamza, S. & Skelton, H. Histologic features in primary cutaneous squamous cell carcinomas in immunocompromised patients focusing on organ transplant patients. *Dermatol Surg* **30**, 634–641 (2004).
25. Yu, X. & Li, Z. The role of miRNAs in cutaneous squamous cell carcinoma. *J Cell Mol Med* **20**, 3–9 (2016).
26. LeBoeuf, N. R. & Schmults, C. D. Update on the management of high-risk squamous cell carcinoma. *Semin Cutan Med Surg* **30**, 26–34 (2011).
27. Schmults, C. D., Karia, P. S., Carter, J. B., Han, J. & Qureshi, A. A. Factors predictive of recurrence and death from cutaneous squamous cell carcinoma: a 10-year, single-institution cohort study. *JAMA Dermatol* **149**, 541–547 (2013).
28. Benjamin, C. L., Melnikova, V. O. & Ananthaswamy, H. N. P53 protein and pathogenesis of melanoma and nonmelanoma skin cancer. *Adv Exp Med Biol* **624**, 265–282 (2008).
29. Zavdy, O. *et al.* Cutaneous Squamous Cell Carcinoma in Immunocompromised Patients-A Comparison between Different Immunomodulating Conditions. *Cancers (Basel)* **15**, 1764 (2023).
30. Ong, C. S., Keogh, A. M., Kossard, S., Macdonald, P. S. & Spratt, P. M. Skin cancer in Australian heart transplant recipients. *J Am Acad Dermatol* **40**, 27–34 (1999).

31. Tam, S. *et al.* Association of Immunosuppression With Outcomes of Patients With Cutaneous Squamous Cell Carcinoma of the Head and Neck. *JAMA Otolaryngol Head Neck Surg* **146**, 128–135 (2020).
32. Abikhair, M. *et al.* Cyclosporine A immunosuppression drives catastrophic squamous cell carcinoma through IL-22. *JCI Insight* **1**, e86434 (2016).
33. Muellenhoff, M. W. & Koo, J. Y. Cyclosporine and skin cancer: an international dermatologic perspective over 25 years of experience. A comprehensive review and pursuit to define safe use of cyclosporine in dermatology. *Journal of Dermatological Treatment* **23**, 290–304 (2012).
34. Paul, C. F. *et al.* Risk of malignancies in psoriasis patients treated with cyclosporine: a 5 y cohort study. *J Invest Dermatol* **120**, 211–216 (2003).
35. Matsuda, S. & Koyasu, S. Mechanisms of action of cyclosporine. *Immunopharmacology* **47**, 119–125 (2000).
36. Euvrard, S., Ulrich, C. & Lefrancois, N. Immunosuppressants and Skin Cancer in Transplant Patients: Focus on Rapamycin. *Dermatol Surg* **30**, 628–633 (2004).
37. Watson, C. J. E. & Dark, J. H. Organ transplantation: historical perspective and current practice. *Br J Anaesth* **108 Suppl 1**, i29-42 (2012).
38. Worst, P. L. & Boukamp, P. CsA is promoting tumor-like invasion in a long-term human skin equivalent. (Heinrich Heine University, Düsseldorf, 2019).
39. Lin, Y. *et al.* NFAT signaling dysregulation in cancer: Emerging roles in cancer stem cells. *Biomedicine & Pharmacotherapy* **165**, 115167 (2023).
40. Lee, H., Myoung, H. & Kim, S. M. Review of two immunosuppressants: tacrolimus and cyclosporine. *JKAOMS* **49**, 311–323 (2023).
41. Nourmohammadi, K., Bayrami, A., Naderi, R. & Shirpoor, A. Cyclosporine A induces cardiac remodeling through TGF-β/Smad3/miR-29 signaling pathway and alters gene expression of

miR-30b-5p/CaMKIIδ isoforms pathways: alleviating effects of moderate exercise. *Mol Biol Rep* **50**, 5859–5870 (2023).

42. Bibee, K. *et al.* Cutaneous squamous cell carcinoma in the organ transplant recipient. *Oral Oncol* **103**, 104562 (2020).
43. Barnes, B. M., Shyne, A., Gunn, D. A., Griffiths, C. E. M. & Watson, R. E. B. Epigenetics and Ultraviolet Radiation: Implications for Skin Ageing and Carcinogenesis. *Skin Health and Disease* **4**, ski2.410 (2024).
44. He, M., Raftrey, B. & Hsu, Y.-C. Epigenetic fun(ction) in the sun. *Developmental Cell* **56**, 2537–2539 (2021).
45. Caroti, L. *et al.* Conversion from calcineurin inhibitors to everolimus with low-dose cyclosporine in renal transplant recipients with squamous cell carcinoma of the skin. *Transplant Proc* **44**, 1926–1927 (2012).
46. Guba, M., Graeb, C., Jauch, K.-W. & Geissler, E. K. Pro- and anti-cancer effects of immunosuppressive agents used in organ transplantation. *Transplantation* **77**, 1777–1782 (2004).
47. Pflugrad, H. *et al.* Brain function and metabolism in patients with long-term tacrolimus therapy after kidney transplantation in comparison to patients after liver transplantation. *PLoS One* **15**, e0229759 (2020).
48. Yang, J. *et al.* Guidelines and definitions for research on epithelial–mesenchymal transition. *Nat Rev Mol Cell Biol* **21**, 341–352 (2020).
49. Nieto, M. A., Huang, R. Y.-J., Jackson, R. A. & Thiery, J. P. EMT: 2016. *Cell* **166**, 21–45 (2016).
50. Kalluri, R. & Weinberg, R. A. The basics of epithelial-mesenchymal transition. *J. Clin. Invest.* **119**, 1420–1428 (2009).

51. De Visser, K. E. & Joyce, J. A. The evolving tumor microenvironment: From cancer initiation to metastatic outgrowth. *Cancer Cell* **41**, 374–403 (2023).

52. Lamouille, S., Xu, J. & Derynck, R. Molecular mechanisms of epithelial–mesenchymal transition. *Nat Rev Mol Cell Biol* **15**, 178–196 (2014).

53. Kalluri, R. & Neilson, E. G. Epithelial-mesenchymal transition and its implications for fibrosis. *J. Clin. Invest.* **112**, 1776–1784 (2003).

54. Xie, Y., Wang, X., Wang, W., Pu, N. & Liu, L. Epithelial-mesenchymal transition orchestrates tumor microenvironment: current perceptions and challenges. *J Transl Med* **23**, 386 (2025).

55. Hoch, C. C., Stögbauer, F. & Wollenberg, B. Unraveling the Role of Epithelial–Mesenchymal Transition in Adenoid Cystic Carcinoma of the Salivary Glands: A Comprehensive Review. *Cancers* **15**, 2886 (2023).

56. Schardt, L. The impact of Cyclosporine A on human epidermal keratinocytes. https://doi.org/10.11588/HEIDOK.00023271 (2017) doi:10.11588/HEIDOK.00023271.

57. Walsh, S. B. *et al.* Cyclosporine a mediates pathogenesis of aggressive cutaneous squamous cell carcinoma by augmenting epithelial-mesenchymal transition: Role of TGFβ signaling pathway. *Molecular Carcinogenesis* **50**, 516–527 (2011).

58. Arumugam, A. *et al.* Combined inhibition of p38 and Akt signaling pathways abrogates cyclosporine A-mediated pathogenesis of aggressive skin SCCs. *Biochemical and Biophysical Research Communications* **425**, 177–181 (2012).

59. Zhou, Q. *et al.* Melanoma-associated fibroblasts in tumor-promotion flammation and antitumor immunity: novel mechanisms and potential immunotherapeutic strategies. *Human Molecular Genetics* **33**, 1186–1193 (2024).

60. Van Hove, L. & Hoste, E. Activation of Fibroblasts in Skin Cancer. *Journal of Investigative Dermatology* **142**, 1026–1031 (2022).

61. Belviso, I. *et al.* The Role of Fibroblasts in Melanoma Development: From Tumor Microenvironment Remodeling to Pre-Metastatic Niche Formation. *Int J Mol Sci* **26**, 6132 (2025).
62. Liang, D. *et al.* Targeting extracellular matrix through phytochemicals: a promising approach of multi-step actions on the treatment and prevention of cancer. *Front. Pharmacol.* **14**, 1186712 (2023).
63. Winkler, J., Abisoye-Ogunniyan, A., Metcalf, K. J. & Werb, Z. Concepts of extracellular matrix remodelling in tumour progression and metastasis. *Nat Commun* **11**, 5120 (2020).
64. Islam, M., Jones, S. & Ellis, I. Role of Akt/Protein Kinase B in Cancer Metastasis. *Biomedicines* **11**, 3001 (2023).
65. Zhao, J., Zeng, X., Song, P., Wu, X. & Shi, H. AKT1 as the PageRank hub gene is associated with melanoma and its functional annotation is highly related to the estrogen signaling pathway that may regulate the growth of melanoma. *Oncology Reports* **36**, 2087–2093 (2016).
66. Cho, J. H. *et al.* AKT1 Activation Promotes Development of Melanoma Metastases. *Cell Rep* **13**, 898–905 (2015).
67. Kwon, H.-K. *et al.* Transcription factor NFAT1 controls allergic contact hypersensitivity through regulation of activation induced cell death program. *Sci Rep* **6**, 19453 (2016).
68. Alrefai, H. *et al.* NFATc1 supports imiquimod-induced skin inflammation by suppressing IL-10 synthesis in B cells. *Nat Commun* **7**, 11724 (2016).
69. Baba, A. B. *et al.* Transforming Growth Factor-Beta (TGF-β) Signaling in Cancer-A Betrayal Within. *Front. Pharmacol.* **13**, 791272 (2022).
70. Shi, X. *et al.* TGF-β signaling in the tumor metabolic microenvironment and targeted therapies. *J Hematol Oncol* **15**, 135 (2022).

71. Serrano-Gomez, S. J., Maziveyi, M. & Alahari, S. K. Regulation of epithelial-mesenchymal transition through epigenetic and post-translational modifications. *Mol Cancer* **15**, 18 (2016).
72. Tanabe, S., Aoyagi, K., Yokozaki, H. & Sasaki, H. Gene expression signatures for identifying diffuse-type gastric cancer associated with epithelial-mesenchymal transition. *International Journal of Oncology* **44**, 1955–1970 (2014).
73. Lu, X. *et al.* Identification of ATF3 as a novel protective signature of quiescent colorectal tumor cells. *Cell Death Dis* **14**, 676 (2023).
74. Imagawa, M. *et al.* Epithelial-to-mesenchymal transition, inflammation, subsequent collagen production, and reduced proteinase expression cooperatively contribute to cyclosporin-A-induced gingival overgrowth development. *Front. Physiol.* **14**, 1298813 (2023).
75. Fang, W. *et al.* [Role of matrix metalloproteinases (MMPs) in tumor invasion and metastasis: serial studies on MMPs and TIMPs]. *Beijing Da Xue Xue Bao Yi Xue Ban* **35**, 441–443 (2003).
76. Liu, B. *et al.* Immunolocalization of MMP9 and MMP2 in osteolytic metastasis originating from MDA-MB-231 human breast cancer cells. *Molecular Medicine Reports* **14**, 1099–1106 (2016).
77. Tölle, R. C. & Dengjel, J. Effects of the Extracellular Matrix on the Proteome of Primary Skin Fibroblasts. *Methods Mol Biol* **1993**, 193–204 (2019).
78. Shi, L., Dong, N., Fang, X. & Wang, X. Regulatory mechanisms of TGF-β1-induced fibrogenesis of human alveolar epithelial cells. *J Cell Mol Med* **20**, 2183–2193 (2016).
79. Glick, A. B. The Role of TGFβ Signaling in Squamous Cell Cancer: Lessons from Mouse Models. *J Skin Cancer* **2012**, 249063 (2012).
80. Nakao, A. *et al.* TGF-beta receptor-mediated signalling through Smad2, Smad3 and Smad4. *EMBO J* **16**, 5353–5362 (1997).

81. Liao, J. *et al.* Cross-Talk between the TGF-β and Cell Adhesion Signaling Pathways in Cancer. *Int. J. Med. Sci.* **21**, 1307–1320 (2024).

82. Boukamp, P. *et al.* Normal keratinization in a spontaneously immortalized aneuploid human keratinocyte cell line. *J Cell Biol* **106**, 761–771 (1988).

83. Plitta-Michalak, B. *et al.* Development and characterisation of an irradiation device for biomedical studies covering the solar spectrum with individual regulated spectral bands. *Photochem Photobiol Sci* **21**, 1701–1717 (2022).

84. Ponchio, L. *et al.* Mitomycin C as an alternative to irradiation to inhibit the feeder layer growth in long-term culture assays. *Cytotherapy* **2**, 281–286 (2000).

85. Gordon Smyth [Cre, A. limma. Bioconductor https://doi.org/10.18129/B9.BIOC.LIMMA (2017).

86. Flatschacher, D., Speckbacher, V. & Zeilinger, S. qRAT: an R-based stand-alone application for relative expression analysis of RT-qPCR data. *BMC Bioinformatics* **23**, 286 (2022).

87. Berndt, N. *et al.* The Akt activation inhibitor TCN-P inhibits Akt phosphorylation by binding to the PH domain of Akt and blocking its recruitment to the plasma membrane. *Cell Death Differ* **17**, 1795–1804 (2010).

88. Saigal, S. *et al.* Evidence of differential risk for posttransplantation malignancy based on pretransplantation cause in patients undergoing liver transplantation. *Liver Transpl* **8**, 482–487 (2002).

89. Sommerer, C., Schnitzler, P., Meuer, S., Zeier, M. & Giese, T. Pharmacodynamic monitoring of cyclosporin A reveals risk of opportunistic infections and malignancies in renal transplant recipients 65 years and older. *Ther Drug Monit* **33**, 694–698 (2011).

90. Flockhart, R. J., Diffey, B. L., Farr, P. M., Lloyd, J. & Reynolds, N. J. NFAT regulates induction of COX-2 and apoptosis of keratinocytes in response to ultraviolet radiation exposure. *FASEB J* **22**, 4218–4227 (2008).
91. Liu, H. *et al.* Ultraviolet B Inhibits Skin Wound Healing by Affecting Focal Adhesion Dynamics. *Photochem Photobiol* **91**, 909–916 (2015).
92. Wiegand, C., Hipler, U.-C., Elsner, P. & Tittelbach, J. Keratinocyte and Fibroblast Wound Healing In Vitro Is Repressed by Non-Optimal Conditions but the Reparative Potential Can Be Improved by Water-Filtered Infrared A. *Biomedicines* **9**, 1802 (2021).
93. Sarkar, M. *et al.* Cancer-associated fibroblasts: The chief architect in the tumor microenvironment. *Front. Cell Dev. Biol.* **11**, 1089068 (2023).
94. Xiang, X. *et al.* Cancer-associated fibroblasts: Vital suppressors of the immune response in the tumor microenvironment. *Cytokine & Growth Factor Reviews* **67**, 35–48 (2022).
95. Alba-Castellón, L. *et al.* Snail1-Dependent Activation of Cancer-Associated Fibroblast Controls Epithelial Tumor Cell Invasion and Metastasis. *Cancer Research* **76**, 6205–6217 (2016).
96. Manabe, T., Park, H. & Minami, T. Calcineurin-nuclear factor for activated T cells (NFAT) signaling in pathophysiology of wound healing. *Inflamm Regen* **41**, 26 (2021).
97. Dotto, G. P. Calcineurin signaling as a negative determinant of keratinocyte cancer stem cell potential and carcinogenesis. *Cancer Res* **71**, 2029–2033 (2011).
98. Tamura, K. *et al.* Stress response gene ATF3 is a target of c-myc in serum-induced cell proliferation. *EMBO J* **24**, 2590–2601 (2005).
99. Hai, T., Wolfgang, C. D., Marsee, D. K., Allen, A. E. & Sivaprasad, U. ATF3 and stress responses. *Gene Expr* **7**, 321–335 (1999).

100. Dziunycz, P. J. *et al.* The Oncogene ATF3 Is Potentiated by Cyclosporine A and Ultraviolet Light A. *Journal of Investigative Dermatology* **134**, 1998–2004 (2014).

101. Jamal, S. & Schneider, R. J. UV-induction of keratinocyte endothelin-1 downregulates E-cadherin in melanocytes and melanoma cells. *J. Clin. Invest.* **110**, 443–452 (2002).

102. Hung, C.-F., Chiang, H.-S., Lo, H.-M., Jian, J.-S. & Wu, W.-B. E-cadherin and its downstream catenins are proteolytically cleaved in human HaCaT keratinocytes exposed to UVB. *Exp Dermatol* **15**, 315–321 (2006).

103. Dai, Q. *et al.* Vorinostat attenuates UVB-induced skin senescence by modulating NF-κB and mTOR signaling pathways. *Sci Rep* **15**, 10905 (2025).

104. Dziunycz, P. *et al.* Squamous cell carcinoma of the skin shows a distinct microRNA profile modulated by UV radiation. *J Invest Dermatol* **130**, 2686–2689 (2010).

105. Richardson, L., Wilcockson, S. G., Guglielmi, L. & Hill, C. S. Context-dependent TGFβ family signalling in cell fate regulation. *Nat Rev Mol Cell Biol* **24**, 876–894 (2023).

106. Smith, A. L., Robin, T. P. & Ford, H. L. Molecular Pathways: Targeting the TGF-β Pathway for Cancer Therapy. *Clinical Cancer Research* **18**, 4514–4521 (2012).

107. Onoue, S., Kobayashi, T., Takemoto, Y., Sasaki, I. & Shinkai, H. Induction of matrix metalloproteinase-9 secretion from human keratinocytes in culture by ultraviolet B irradiation. *Journal of Dermatological Science* **33**, 105–111 (2003).

108. Kim, D. J., Iwasaki, A., Chien, A. L. & Kang, S. UVB-mediated DNA damage induces matrix metalloproteinases to promote photoaging in an AhR- and SP1-dependent manner. *JCI Insight* **7**, e156344 (2022).

109. Su, M. *et al.* Role of the p53-TRPM1/miR-211-MMP9 axis in UVB-induced human melanocyte migration and its potential in repigmentation. *Int J Mol Med* https://doi.org/10.3892/ijmm.2020.4478 (2020) doi:10.3892/ijmm.2020.4478.

110. Bergholz, J. S. & Zhao, J. J. How Compensatory Mechanisms and Adaptive Rewiring Have Shaped Our Understanding of Therapeutic Resistance in Cancer. *Cancer Research* **81**, 6074–6077 (2021).

111. Koike, M., Ninomiya, Y. & Koike, A. Characterization of ATF3 induction after ionizing radiation in human skin cells. *J Radiat Res* **46**, 379–385 (2005).

112. Zu, T. *et al.* Up-Regulation of Activating Transcription Factor 3 in Human Fibroblasts Inhibits Melanoma Cell Growth and Migration Through a Paracrine Pathway. *Front Oncol* **10**, 624 (2020).

113. Kang, W. *et al.* Post-EMT: Cadherin-11 mediates cancer hijacking fibroblasts. Preprint at https://doi.org/10.7554/eLife.87423.1 (2023).

114. Liu, S., Ren, J. & Ten Dijke, P. Targeting TGFβ signal transduction for cancer therapy. *Sig Transduct Target Ther* **6**, 8 (2021).

115. Deng, Z. *et al.* TGF-β signaling in health, disease and therapeutics. *Sig Transduct Target Ther* **9**, 61 (2024).

116. Xue, M. & Jackson, C. J. Autocrine Actions of Matrix Metalloproteinase (MMP)-2 Counter the Effects of MMP-9 to Promote Survival and Prevent Terminal Differentiation of Cultured Human Keratinocytes. *Journal of Investigative Dermatology* **128**, 2676–2685 (2008).

117. Legrand, C. *et al.* Airway epithelial cell migration dynamics. MMP-9 role in cell-extracellular matrix remodeling. *J Cell Biol* **146**, 517–529 (1999).

118. Wang, Y. *et al.* The role of matrix metalloproteinase 9 in fibrosis diseases and its molecular mechanisms. *Biomedicine & Pharmacotherapy* **171**, 116116 (2024).

Acknowledgment

This work would not have been possible without the guidance, encouragement, and support I received throughout this journey. I would like to take this opportunity to express my sincere gratitude to all those who contributed to this work in various ways.

First and foremost, I am deeply grateful to Dr. Beate Volkmer, Dr. Rüdiger Greinert, and Elbe Klinikum Buxtehude for granting me the opportunity to conduct my thesis at such an esteemed institution. Their efforts in fostering an environment that encouraged learning and skill development in Molecular and Cell Biology were invaluable. I am also sincerely thankful to Prof. Dr. Petra Boukamp for her collaborative contributions and continuous support throughout the course of this project.

I owe special thanks to Prof. Dr. Julien Béthune, who took on the responsibility of being my internal supervisor. His steady support and thoughtful guidance made a significant difference throughout my master's studies and the completion of this thesis.

My deepest appreciation goes to Dr. Sarah Degenhardt for supervising this work and for her careful planning, insightful advice, constructive feedback, and continuous guidance throughout the experimental and analytical stages. I also wish to express my gratitude to Dipl.-Ing. Stefan Henning and Dr. I-Peng Chen for their dedication, assistance, and valuable contributions to the progress of the project on which this thesis is based.

I would like to thank Dr. Mouna Mhamdi-Ghodbani, Dr. Marc Bender, and Huda Jama for their encouragement during this journey, as well as the laboratory team, especially Sylke Engel-Haskiris, Stefanie Balk, and Rebecca Keck, for their technical expertise, collaborative spirit, and for creating a stimulating laboratory environment. Their patience, support, and kindness helped me persevere through the challenges I faced along the way.

Lastly, I am deeply grateful for the meaningful connections I was able to form during my time here. The warmth, collegiality, and camaraderie of the entire Molecular Cell Biology team made this journey not only productive but also truly enjoyable. Working alongside such an inspiring group of people has been an honor, and I will always cherish this experience.

Statutory Declaration

I hereby declare that the present study is my own original work and that I have properly acknowledged all assistance and support received from others. Furthermore, I confirm that neither this work nor any part of it has been submitted by me or any other individual to another university as part of a formal degree requirement. All intellectual property belonging to others has been clearly cited.

All secondary literature and other sources used are properly referenced and listed in the references section. This includes graphic illustrations, images, and internet sources.

I consent to my work being electronically stored and anonymously submitted for plagiarism checking. I understand that this thesis cannot be graded unless this declaration is signed.

Hamburg, 15 October 2025

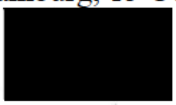

Elizabeth Bella Agustya